Contents lists available at ScienceDirect

Chemical Geology

journal homepage: www.elsevier.com/locate/chemgeo

# Episodic hydrothermal alteration recorded by microscale oxygen isotope analysis of white mica in the Larderello-Travale Geothermal Field, Italy

Florian Bulle[a,*], Daniela Rubatto[a,b], Giovanni Ruggieri[c], Cindy Luisier[b], Igor M. Villa[a,d], Lukas Baumgartner[b]

[a] Institut für Geologie, University of Bern, Baltzerstrasse 1+3, CH-3012 Bern, Switzerland
[b] Institut des Sciences de la Terre, University of Lausanne, Géopolis, CH-1015 Lausanne, Switzerland
[c] CNR-Instituto di Geoscienze e Georisorse, Via La Pira 4, I-50121 Firenze, Italy
[d] Centro Universitario Datazioni e Archeometria, University of Milano Bicocca, Piazza della Scienza 4, I-20126 Milano, Italy

ARTICLE INFO

Editor: Michael E. Boettcher

*Keywords:*
In-situ stable isotope analysis
Geothermal system
Secondary Ion Mass Spectrometry
Hydrothermal alteration
K-Ar white mica geochronology

ABSTRACT

Microscale oxygen isotope analysis ($^{18}O/^{16}O$) of minerals can identify distinct events of fluid-rock interaction. This method is, however, still limited to a few major and accessory minerals of which most are anhydrous minerals. We present the systematic study of oxygen isotope distribution in white mica by Secondary Ion Mass Spectrometry (SIMS). Texturally and chemically distinct white mica populations in granitic and contact metamorphic rocks from the Larderello-Travale geothermal field (LTGF), Italy, record stages of magmatic crystallization, metamorphic-hydrothermal replacement and fluid-rock interaction. The large range in intra- and inter-grain white mica $\delta^{18}O$ values between 1 and 14‰ reflects varying protoliths and degrees of fluid-mineral interaction at variable temperatures (180–450 °C present-day temperatures; p.d.T.). This variability reflects the large-scale circulation of both (1) magmatic, *syn*-intrusive to early contact metamorphic hydrothermal fluids with high-$\delta^{18}O$ values, and (2) meteoric fluids with $\delta^{18}O$ values of −7‰ during a post-intrusive, late hydrothermal stage.

Metasedimentary rocks from the upper reservoir contain distinct white mica populations occurring in close proximity (μm-scale), including detrital grains ($\delta^{18}O$ = 12–14‰; high Na, low Mg), partially altered white mica ($\delta^{18}O$ = 8–9‰) and late hydrothermal white mica (1–6‰; low Na, mid Mg). The late hydrothermal white mica has similar $\delta^{18}O$ values to other secondary minerals and is in equilibrium with meteoric-dominated fluids with a $\delta^{18}O$ of −6 to 0.5‰, which circulated in the late hydrothermal stage. Downhole towards the lower reservoir, white mica from two contact metamorphic micaschist samples shows either (1) homogeneous $\delta^{18}O$ values of ca. 9‰ likely due to recrystallization in the contact metamorphic hydrothermal stage (T ca. 600 °C), or (2) a large spread in $\delta^{18}O$ from 2 to 12‰ within and across grains of variable texture and chemistry in the host rock and a cross-cutting quartz-white mica vein (ca. 300 °C, present day temperature; hereafter p.d.T.). This contrasting $\delta^{18}O$ signature of white mica is also recorded in granite cored at up to 4.6 km depth. The Carboli granite contains white mica with a homogeneous magmatic $\delta^{18}O$ of 10 ± 0.6‰, whereas older granite samples from Radicondoli have magmatic to hydrothermal white micas that vary in $\delta^{18}O$ from 4 to 10‰. A pronounced intra-grain $\delta^{18}O$ variability of up to 6‰ occurs in white mica domains with higher Fe-Mg-Ti halos around inclusions of chloritized biotite, as a result of interaction with dominantly meteoric fluids that infiltrated to depths of at least 4.6 km. In the Porto Azzurro granite on Elba, Italy, altered white mica has $\delta^{18}O$ values of 2.6‰ down from 10‰ in unaltered grains.

The distribution of oxygen isotope ratios in white mica is thus firstly a result of pervasive versus selective fluid alteration (at depth, sample and grain scale). Secondly, the actual preservation of these μm-scale variabilities indicates that volume diffusion is not detectable at microscale at p.d.T at or below 350 °C where most of the heterogeneous white mica is found. Selective, sample- and grain-scale fluid penetration occurs episodically and anisotropically, on micro- and megascale, along faults, fractures and cleavages, producing lower $\delta^{18}O$ white mica at various times in zones of higher secondary permeability and active hydrothermal fluid circulation.

* Corresponding author.
*E-mail address:* florian.bulle@geo.unibe.ch (F. Bulle).

https://doi.org/10.1016/j.chemgeo.2019.119288
Received 21 February 2019; Received in revised form 14 August 2019; Accepted 28 August 2019

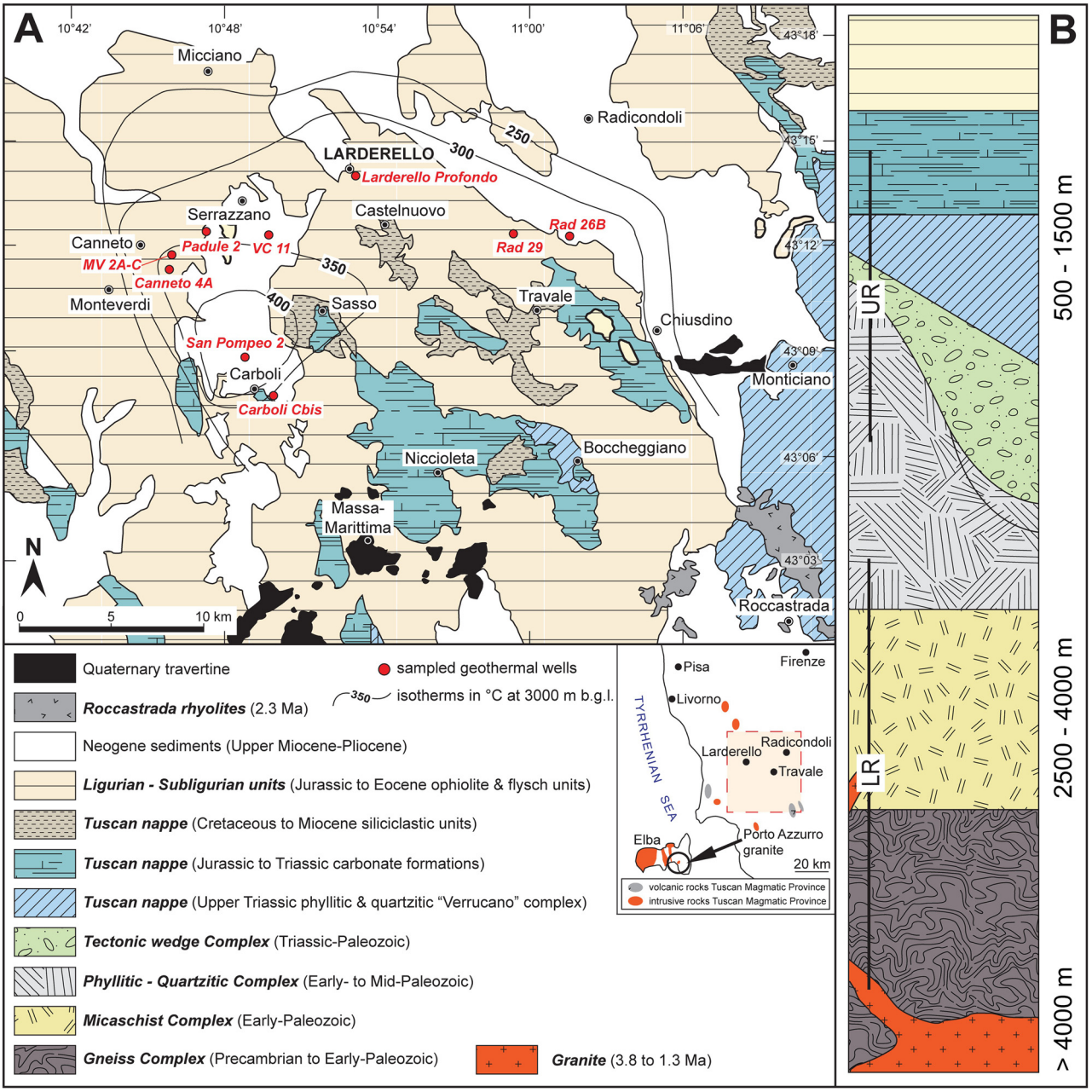


**Fig. 1.** A – Simplified geological map of the Larderello-Travale geothermal field with sampled geothermal wells and the isotherms at 3000 m (b.g.l.) in °C (after Carella et al., 2000; Gianelli and Ruggieri, 2002). Inset in A – Simplified map of the distribution of igneous rocks belonging to the Tuscan Magmatic Province between the island of Elba in the East and Firenze in the West (after Dini et al., 2005); the rectangle denotes the LTGF. B – Schematic lithostratigraphic column of the LTGF with the major lithologies and approximate depths of the Upper Reservoir (UR) and Lower Reservoir (LR) (adjusted after Bertini et al., 2006).

## 1. Introduction

Oxygen isotopes have been applied extensively to trace fluid-rock interaction in volcanic, igneous and metamorphic systems (e.g. Taylor, 1977; Criss and Taylor, 1986; Taylor and Sheppard, 1986; Valley, 1986; Eiler, 2001; Bindeman, 2008). Interaction between components with a distinct isotopic signature occurs commonly in the crust, where fluids and melts interact with or assimilate country rocks in various proportions, and the $\delta^{18}O$ composition of the end product (rock or mineral) can be used to trace its source (e.g. Taylor and Sheppard, 1986; Eiler et al., 1993; Baumgartner and Valley, 2001; Eiler, 2001; Bindeman, 2008). With the advances in microscale analysis, especially high-resolution Secondary Ion Mass Spectrometry (SIMS), $^{18}O/^{16}O$ data can be precisely and accurately collected on μm-scale. The major advantage of microscale, in situ analysis, is the ability to resolve individual mineral growth zones and other micro-features and relate those to specific igneous, metamorphic or hydrothermal episodes (e.g. Bindemann, 2008; Ferry et al., 2014). Most studies on igneous rocks so far have been focused on refractory mineral phases such as olivine, quartz and zircon, which are chemically simple, relatively resistant to secondary isotope exchange and often preserve initial isotopic compositions.

However, there is a growing need to expand the microanalytical approach to reactive-water bearing minerals. Studies of in-situ oxygen isotope analysis on major hydrous minerals are so far limited to serpentine minerals (Scicchitano et al., 2018; Rouméjon et al., 2018) and potential biotite reference materials (Siron et al., 2017). White mica on the other hand, is used regularly for geothermobarometry and geochronology (e.g. O'Neil and Taylor, 1969; Bottinga and Javoy, 1973;

Villa et al., 1987; Zheng, 1993; Villa et al., 2006; Airaghi et al., 2017), and occurs in many crustal metamorphic and hydrothermal systems, but has not been investigated specifically for its microscale $^{18}O/^{16}O$ distribution. Early experimental and empirical data suggests that white mica is almost as reactive to oxygen isotope exchange and re-equilibration as feldspar. This reactivity of white mica has been recorded from mid-crustal conditions down to a temperature of around 300 °C (Fortier and Giletti, 1991; Chacko et al., 1996; Kohn and Valley, 1998), although early field data from the Larderello-Travale geothermal field (LTGF) seems to show a low reactivity of white mica (Petrucci et al., 1994).

To investigate the oxygen isotope variations of white mica, and specifically its ability to resist $^{18}O/^{16}O$ exchange under hydrothermal conditions in the upper crust, we present a systematic, SIMS micro-analytical study of in situ oxygen isotopes in white mica in rocks from the LTGF. Two main characteristics make this geothermal field an excellent study site: (1) the wealth of geochemical and isotopic information on rocks and interacting hydrothermal waters, and (2) the widespread occurrence of white mica in most rock types, from the granitic intrusions to the metasedimentary country rocks.

In light of the ongoing search for an exploitable deep-seated geothermal reservoir at Larderello (Gianelli and Ruggieri, 2002; Bertini et al., 2006; Saccorotti et al., 2014) we investigated samples from different lithologies (granite intrusions, contact metamorphic rocks, hydrothermal veins, and phyllites) cored at depths between 581 and 4600 m below ground level (b.g.l.). Corresponding major and trace element chemical analyses and $^{39}Ar$-$^{40}Ar$ age dating of selected white mica samples complement the oxygen isotope data. By combining in-situ $\delta^{18}O$ values with mineral chemistry and new Ar isotope data measured on white micas from a group of vertically and spatially distributed shallow and deep wells, we aim to characterize white mica – fluid interaction, and the temporal and spatial evolution of the circulating hydrothermal fluids. Different white mica populations, from different spatial positions within the stratigraphy of the LTGF preserve intra- and inter-grain $^{18}O/^{16}O$-variations, as well as $^{39}Ar$-$^{40}Ar$ formation ages respective of their magmatic, metamorphic, detrital, or authigenic formation, but also record interaction with hydrothermal fluids dominant in the early or late evolution of the LTGF. These datasets are combined to gain insight in the processes that reset oxygen isotope signatures of white mica as well as its retentivity.

## 2. Previous studies

### 2.1. Geological setting

The Larderello-Travale geothermal field (Tuscany, Italy; Fig. 1) is a steam-dominated geothermal system that has been commercially exploited for electricity production for over 100 years (Parri and Lazzeri, 2016). The LTGF is located in an area characterized by thinned continental crust (ca. 23 km) and it owes its longevity to locally very high heat flows (up to 1000 mW $m^{-2}$, Bertini et al., 2006) and high geothermal gradients of > 100 °C/km up to a maximum of 300 °C/km (Batini et al., 1985). Peraluminous acidic intrusions (primarily monzo- and syenogranites) of Pliocene to Pleistocene ages have been found in boreholes at 3–4 km depth (Dini et al., 2005), whereas a partially molten granitic body likely occurs below the present-day exploited reservoir (Gianelli et al., 1997).

The intrusive rocks of the LTGF and Elba are part of the Tuscan Magmatic Province (Fig. 1A; Dini et al., 2005 and references therein). Mineralogical, chemical and isotope data suggest a crustal origin for the granite intrusions of the LTGF by melting of high-$\delta^{18}O$, biotite- and muscovite-rich, pelitic source rocks (Taylor and Turi, 1976; Dini et al., 2005; Farina et al., 2018). Intrusion and emplacement occurred episodically between 3.8 and 1.3 Ma (Batini et al., 1985; Villa and Puxeddu, 1994; Villa et al., 1997; Villa et al., 2001; Farina et al., 2018) within the Micaschist and Gneiss Complexes (Fig. 1B) of the Precambrian to Paleozoic basement (Cavarretta et al., 1980; Pandeli et al., 2005; Bertini et al., 2006). The low- to medium-high grade contact metamorphic parageneses (1.5–2 kbar, 500–650 °C) that developed after granite emplacement include biotite, cordierite, andalusite, sometimes sillimanite, and rarely corundum (Cavarretta et al., 1980; Gianelli and Ruggieri, 2002; Musumeci et al., 2002; Rossetti et al., 2008). According to Pandeli et al. (2005) and Bertini et al. (2006), the contact metamorphic aureole developed in the Micaschist and Gneiss Complexes and in the overlying Phyllitic-Quartzitic Complex (Fig. 1B). Carella et al. (2000) and Musumeci et al. (2002) propose a different interpretation for the deep metamorphic complexes of the LTGF suggesting that the deep medium- and high-grade metamorphic rocks do not represent remnants of an older poly-metamorphic basement, but result from the development of thermal aureoles in low-grade metamorphic rocks (i.e. the Phyllitic-Quartzitic Complex), associated with the emplacement of the Neogene granites.

The metamorphic basement is overlain by a Tectonic Wedges Complex (Fig. 1B), mainly composed of slices of Upper Triassic carbonate and evaporites, Triassic quartzite and phyllite metasiliciclastics ("Verrucano"), and metasediments of the Phyllitic-Quartzitic Complex (Pandeli et al., 2005). Above the Tectonic Wedge Complex are units of the Tuscan Nappe, commonly consisting from bottom to top of Upper Triassic shallow marine carbonate and evaporitic sequences, Jurassic limestone and Cenozoic siliciclastic intervals (Cavarretta et al., 1980; Puxeddu et al., 1984). The cover of the LTGF consists of Upper Jurassic–Eocene Ligurian flysch with minor ophiolite rocks, sub-Ligurian flysch and Neogene lacustrine and marine sediments (Bertini et al., 2006).

In the LTGF, the host rocks of the upper geothermal reservoir (UR) are mainly carbonate-evaporite formations of the Tuscan Nappe and of the Tectonic Wedge Complex. The UR has a present-day temperature range of 220–250 °C and was exploited for dry-steam production from 0.5 to 1.5 km depth b.g.l., before the 1980s (Bertini et al., 2006). More recently, productive horizons were discovered in the metamorphic basement at greater depth (i.e. usually between 2 and 4 km b.g.l.) (Barelli et al., 1995; Bertini et al., 2006). This lower reservoir (LR), stores superheated steam in vaporstatic equilibrium with the UR and has temperatures of 300–350 °C, and pressures of about 70 bar at a depth of 3 km (Barelli et al., 1995).

A productive, discontinuous layer within the LR, identified on seismic profiles at depth between 2 and 4 km, termed the "H-horizon", sits on top of the Pliocene granite intrusions and corresponds to the extent of the contact aureole (Bertini et al., 2006; Casini et al., 2010). The H-horizon may thus be the fossil equivalent of the better-known "K-horizon", a high-amplitude seismic reflector at depths between 3 and 6 km that suggests the presence of a (micro)fracture-bound, fluid-rich level on top of younger, Quaternary granite intrusions (Batini et al., 1985; Bertini et al., 2006; Saccorotti et al., 2014). Based on its seismic and rheological characteristics, and fluid inclusion studies, it has been proposed that the K-horizon contains supercritical or super-hot (> 420 °C) fluids and is regarded as a potential deep-seated geothermal reservoir (Gianelli and Ruggieri, 2002; Brogi et al., 2003; Bertini et al., 2006; Boiron et al., 2007; Saccorotti et al., 2014).

Post-collisional extension, especially from the Pliocene onwards, resulted in a network of large low- to high-angle, NW-trending normal faults that extend down to the LR (Brogi et al., 2003; Bellani et al., 2004; Bertini et al., 2006). They dissect the tectonic pile in the LTGF, coalesce to wider shear zones at depth (4–6 km) and are regarded as effective fluid pathways, with high localized secondary permeability, for dual up- and down-flow of convecting fluids (Brogi et al., 2003; Bellani et al., 2004; Liotta et al., 2010).

The eastern part of Elba, intruded by the Porto Azzurro granite (Fig. 1A inset; 5.9 to 5.4 Ma; Maineri et al., 2003), is regarded as an exhumed paleo-analogue of the LTGF that hosted a deep-seated geothermal system. (Taylor and Turi, 1976; Carella et al., 2000; Bertini et al., 2006; Dini et al., 2008; Zucchi et al., 2017).

Understanding fluid circulation (source, flow pattern, recharge, and residence time), as a driver for energy production, is of vital importance for a producing geothermal system such as the LTGF. Numerous mineralogical, stable isotope ($\delta^{18}O$, $\delta D$) and fluid inclusion studies have established and improved the current reservoir model (Batini et al., 1985, D'Amore et al., 1987; Cavarretta and Puxeddu, 1990; Valori et al., 1992; Cathelineau et al., 1994; Petrucci et al., 1993, 1994; Gianelli et al., 1997; Ruggieri and Gianelli, 1999; Ruggieri et al., 1999; Carella et al., 2000; Gianelli and Ruggieri, 2002; Boyce et al., 2003; Dallai et al., 2005). In general, two major stages of hydrothermal fluid alteration are distinguished: (1) an early high-temperature (HT) phase, coeval with the emplacement of the granitic intrusions and the contact metamorphic overprint, with fluids of mostly local magmatic provenance ($\delta^{18}O$ = 11–15‰), and (2) a late to present day low-temperature (LT) hydrothermal stage, dominated by mixing between infiltrating meteoric fluids and deep high-$\delta^{18}O$ fluids which could be residual magmatic fluids and/or a meteoric fluids that undergone oxygen isotope exchange with the host rocks (Petrucci et al., 1993, 1994; D'Amore and Bolognesi, 1994; Gianelli and Ruggieri, 2002; Boyce et al., 2003; Dallai et al., 2005).

### 2.2. Published oxygen isotope data

Stable isotope data ($\delta^{18}O$, $\delta D$, $\delta^{13}C$) from the LTGF are available for a wide range of lithologies, minerals (primary and authigenic), fluid inclusions, dry steam used for energy production, and fluids of variable sources (condensate, reinjection, spring water) (Celati et al., 1973; Panichi et al., 1974; D'Amore et al., 1987; Petrucci et al., 1993, 1994; D'Amore and Bolognesi, 1994; Ruggieri and Gianelli, 1999; Gianelli and Ruggieri, 2002; Boyce et al., 2003; Dallai et al., 2005; Farina et al., 2018). A relevant compilation of $\delta^{18}O$ data for the LTGF is given in Fig. 2, including whole rock $\delta^{18}O$ data for felsic igneous rocks of the Tuscan Magmatic Province and Elba (Taylor and Turi, 1976), as well as an unaltered micaschist from the Northern Appennines (Pontremoli 1 well) with no evidence of post-Alpine contact metamorphism (Gianelli and Ruggieri, 2002).

Published bulk rock $\delta^{18}O$ values span from ca. 3‰ in a micaschist from the LTGF (Petrucci et al., 1993) to ca. 17‰ in a quartz latite from Tolfa, Italy (Taylor and Turi, 1976), whereas bulk mineral $\delta^{18}O$ values range from ca. –1‰ in chlorite (Boyce et al., 2003) to ca. 14.5‰ in quartz from the LTGF (Petrucci et al., 1993, 1994). A large dataset of $\delta^{18}O$ and $\delta D$ values for fluids and steam from the LTGF before re-injection shows a spread of $\delta^{18}O$ values between −7 and 0‰. Two interpretations have been proposed for the $\delta^{18}O$ spread: (1) simple mixing between a primary deep steam of $\delta D$ = 40 ± 2‰ and $\delta^{18}O$ = 0 ± 2‰ and a secondary steam derived from the boiling of fresh waters with $\delta D$ = 40 ± 2‰ and $\delta^{18}O$ = −7‰, (Celati et al., 1973; Panichi et al., 1974; Panichi et al., 1995); (2) mixing between fluids of local meteoric origin (ca. −7‰) and magmatic fluids in the deeper part of the system (ca. 9‰ at San Pompeo 2, 400 °C at 3 km; D'Amore and Bolognesi, 1994; Fig. 2). The primary magmatic fluids, expelled from the crystallizing plutons in the area, have an even higher $\delta^{18}O$ value of 11–15‰ (Fig. 2), due to the heterogeneous, high-$\delta^{18}O$ metasedimentary source of the peraluminous LTGF granite intrusions (Taylor and Turi, 1976; D'Amore and Bolognesi, 1994; Gianelli and Ruggieri, 2002; Farina et al., 2018).

Granites from the LTGF have bulk rock $\delta^{18}O$ values between ca. 6 and 13‰ (Gianelli and Ruggieri, 2002; Fig. 2) and granites from Elba ca. 5 to 12‰ (Taylor and Turi, 1976; Fig. 2). The high $\delta^{18}O$ values record the primary magmatic composition, whereas the low values are interpreted to result from $^{18}O$-depletion through post-crystallization interaction with meteoric fluids (Taylor and Turi, 1976; Taylor, 1977; Criss and Taylor, 1986; Petrucci et al., 1993). Secondary, low-$\delta^{18}O$ chlorite (ca. –1‰) and K-feldspar (ca. 4‰) from a shallow granite (ca. 2.5 km) drilled at Monteverdi in the western part of the LTGF support this interpretation (Boyce et al., 2003).

The metasedimentary successions (phyllite and micaschist of the LR; Fig. 1B) at the LTGF have hydrothermally altered intervals with a low $\delta^{18}O$ of ca. 3‰ in contrast to a value of ca. 12‰ for unaltered phyllite (Petrucci et al., 1993; Gianelli and Ruggieri, 2002). Micaschist intervals in the depth range of 2–3 km that experienced contact metamorphism at temperatures of 500–650 °C have comparable bulk rock $\delta^{18}O$ values from 5 to 11‰, with the highest value in the deepest (ca. 3 km) and hottest sampled well San Pompeo 2 (SP2, ca. 450 °C present-day temperature; p.d.T.; Cavarretta and Puxeddu, 1990). The low bulk rock $\delta^{18}O$ values have been attributed to late-stage interaction with heated fluids of dominantly meteoric origin (Petrucci et al., 1993, 1994; Gianelli and Ruggieri, 2002). The presence of active secondary permeability in the micaschist favours infiltration and channelization of meteoric fluids (Petrucci et al., 1993, 1994).

## 3. Sample characterization

We subsampled 13 drill cuttings and core samples from 9 geothermal wells in the LTGF (Fig. 1A, Table 1). The majority of the samples come from the metamorphic complexes of the LR and from the granitic intrusions below (1.5–4.8 km; Fig. 1B). These include six granite samples, two samples each from the Micaschist and Gneiss Complexes, which have been variably overprinted by contact metamorphism. Metasediment samples from the UR (< 1.5 km; Fig. 1B)

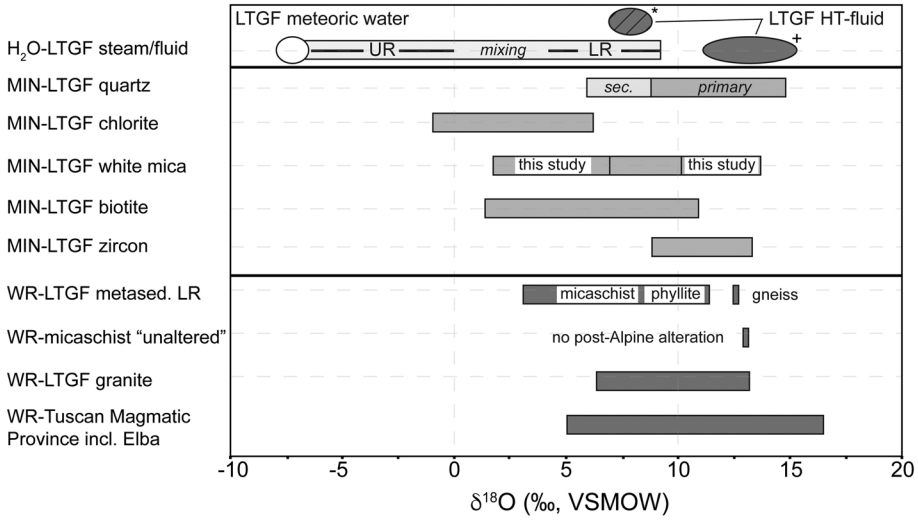


**Fig. 2.** Compilation of $\delta^{18}O$ ‰ literature data for whole rocks, minerals, fluids, and steams from the Upper Reservoir (UR) and Lower Reservoir (LR) of the LTGF. Data for steam and fluid samples is connected by a theoretical mixing line with intermediate compositions (mixing). The highest in-hole measured $\delta^{18}O$ value of 9‰ for steam from the LR comes from the San Pompeo 2 well D'Amore and Bolognesi (1994). Data are from Taylor and Turi (1976), Petrucci et al. (1993, 1994), D'Amore and Bolognesi (1994), Gianelli and Ruggieri (2002), Boyce et al. (2003), Farina et al. (2018). Fields for magmatic – HT fluids for igneous rocks (*) are from Sheppard (1986) and for hypothetical fluids in equilibrium with the igneous rocks with high $\delta^{18}O$ values at the LTGF ($^{+}$) from D'Amore and Bolognesi (1994).

**Table 1**
Petrographic description of samples from Larderello and Elba selected for SIMS $^{18}O/^{16}O$ analyses and $^{40}Ar$–$^{39}Ar$ dating (*).

| Location | Sample ID | Well name | Well no. | Depth (m) | Regional unit | Lithology | Major mineral paragenesis | White mica populations |
|---|---|---|---|---|---|---|---|---|
| Larderello | LP-01* | Larderello profondo | | 581 | "Verrucano unit"-Tuscan Nappe | metasediments (quartzite/phyllite) | qtz-kfs-alb-wm-ep-sul-carb | det - hyd partial - hyd |
| | LP-04 | Larderello profondo | | 1764 | phyllitic-quartzitic complex | metasediments (phyllite) | qtz-kfs-alb-wm-ep-chl-sul | met-1 |
| | MV2A-01 | Monteverdi | 2A | 1871 | phyllitic-quartzitic complex | metasediments (phyllite) | qtz-wm-chl-alb-kfs-ep-sul | det |
| | VC11–01-2a | VC - Serrazzano | 11 | 3191 | gneiss complex | gneiss (contact aureole) | qtz-kfs-plag-bt-wm-sil-and-tur | met-1 |
| | VC11–02-19b | VC-Serrazzano | | | gneiss complex | gneiss (contact aureole) | qtz-kfs-plag-wm-sil-and-tur-chl ± grt | met-2 |
| | SP-01 | San Pompeo | 2 | 3382 | micaschist complex | micaschist (contact aureole) | qtz-alb-kfs-chl-bt-wm-ep-and-sil-sul | met-1 |
| | CT-01* | Canneto | 4A | 3523 | micaschist complex | micaschist (contact aureole) | qtz-kfs-alb-bt-wm-chl-ep-tur-ilm | met-1 - met-2 |
| | Pad2–01* | Padule | 2 | 2782 | phyllitic-quartzitic complex | HT hydrothermal vein crosscutting thermometamorphosed phyllite (contact aureole) | qtz-plag-tur-wm-and-chl | met-2 |
| | CarbA-01 | Carboli C Bis | A | 4204 | granite intrusion | monzogranite | qtz-kfs-plag-bt-wm | mag |
| | CarbA-02 | Carboli C Bis | A | 4304 | granite intrusion | syenogranite | qtz-kfs-plag-bt-wm-crd-tur | mag |
| | RC29–03 | Radicondoli | 29 | 4548 | granite intrusion | monzogranite | qtz-kfs-plag-bt-wm-crd-and-tur | mag |
| | RC26B-01A* | Radicondoli | 26B | 4600 | granite intrusion | monzogranite | qtz-kfs-plag-bt-wm-tur | mag - mag-hyd |
| | RC26B-02E | Radicondoli | | | granite intrusion | monzogranite | qtz-kfs-plag-bt-wm-tur-chl-crd | mag |
| Elba | CR-1 | outcrop | | | Porto Azzurro intrusion | monzogranite (unaltered) | qtz-kfs-plag-bt-wm-tur-chl | mag |
| | CR-2 | outcrop | | | Porto Azzurro intrusion | monzogranite (altered) | qtz-kfs-plag-bt-wm-tur-chl | mag - mag-hyd |

mineral abbreviations: qtz - quartz; kfs - potassium feldspar; plag - plagioclase; bt - biotite; wm - white mica; tit - titanite; tur - tourmaline; chl - chlorite; ep - epidote/allanite; crd – cordierite and - andalusite; sil - sillimanite; grt - garnet; carb - carbonate; sul - sulphide; * samples used for $^{39}Ar$-$^{40}Ar$ dating white mica populations: det - detrital; hyd partial - partially hydrothermally reequilibrated; hyd - late hydrothermal phase; met-1 - regional metamorphic; met-2 - contact metamorphic to early hydrothermal phase; mag - primary magmatic; mag-hyd - altered primary magmatic; see text for further description.

come from the Larderello Profondo and Monteverdi wells and comprise a quartz arenite interval from the Verrucano unit (LP-01) of the Tuscan Nappe. Further downhole we sampled two phyllitic intervals (LP-04, MV2A) from the Phyllitic-Quartzitic Complex. Two additional samples, one altered and one unaltered granite, come from outcrops of the Porto Azzurro pluton on the island of Elba (Maineri et al., 2003), approximately 60 km to the W-SW of the LTGF.

### 3.1. Metasediment samples – Upper Reservoir

Sample LP-01 is a fine-grained, quartz arenite. White mica is embedded in a matrix of quartz, sericite and minor calcite (Fig. 3A). The detrital white micas (hereafter "det") form elongated subhedral crystals along the weakly-defined foliation. Late hydrothermal minerals such as K-feldspar, polycrystalline white mica and pyrite aggregates, as well as epidote, occur together in pockets and small veinlets (Fig. 3B). The hydrothermal white mica population (hereafter "hyd") is anhedral and mostly enclosed by K-feldspar (Fig. 3B).

Phyllite samples LP-04 and MV2A-01, have a similar mineral assemblage to that of LP-01, and are both fine-grained with layers of lepidoblastic white mica, chlorite and minor epidote. These layers are intercalated with granoblastic layers of mostly anhedral quartz and plagioclase, and in LP-04, with pockets of sub- to euhedral epidote and anhedral K-feldspar. Two white mica populations can be texturally distinguished in LP-04 and three in MV2A-01 (Electronic Appendix Fig. A1). Both samples have the foliation-defining, metamorphic white mica (hereafter "met-1"), and the ubiquitous late hydrothermal sericite. MV2A-01 also contains some subhedral, platy, detrital white mica (det) that is oriented perpendicular to the major foliation. This sample is also cross-cut by a hydrothermal quartz veinlet. Parts of the host phyllite in contact with the veinlet ($\leq$5 mm) are strongly altered to chlorite and sericite. Samples from these wells and depths were also used for mineralogical, geochemical and fluid inclusion studies by Puxeddu et al. (1977), Cavarretta et al. (1980) and Ruggieri et al. (1999).

### 3.2. Gneiss and micaschist samples – Lower Reservoir

The two gneiss samples (VC11-01-2a and VC11-02-19b) come from the same well and depth interval and have similar texture and mineralogy (Table 1). White mica (5–10 mod. %) occurs as a subhedral, polycrystalline population (met-1), often closely associated with contact metamorphic andalusite. Minor sericite occurs as alteration, most often around andalusite. Sillimanite is present as fibrolite with apatite, tourmaline and pyrite as other accessory phases. Sample VC11-02-19b is cross-cut by a coarse-grained quartz-K-feldspar-white mica veinlet ($<$ 10 mm thick) with minor amounts of fibrolite and pyrite. Texturally the vein white mica (hereafter "met-2": contact metamorphic to early hydrothermal white mica) is different from the earlier host-rock population of white mica (met-1); it has a larger grain size ($\leq$1 mm vs. $\leq$0.5 mm) and a mostly euhedral shape.

The two micaschist samples (SP-01 and CT-01) come from the same stratigraphic unit but different depths from two geographically close wells (Fig. 1A). Both are variably to strongly overprinted by contact metamorphism according to their spatial position in the thermal aureole. Their mineral assemblage and texture are very similar; lepidoblastic biotite and white mica, strongly altered to chlorite, are intercalated with layers of quartz, K-feldspar and plagioclase with occasional porphyroclastic quartz. Epidote, tourmaline and pyrite occur as minor phases, together with poikilitc, anhedral andalusite in CT-01 (Fig. 3C), and fibrolite in SP-01. The latter sample also has relics of green hornblende. Both samples have two dominant, texturally distinct populations of white mica, a sub- to anhedral, foliation-defining, metamorphic white mica (met-1; Fig. 3C) and the late, hydrothermal stage-dominant sericite. In SP-01, the metamorphic white mica is also tightly intergrown with sub-μm grains of biotite or overgrown by biotite fringes. There are three additional, texturally distinguishable white mica

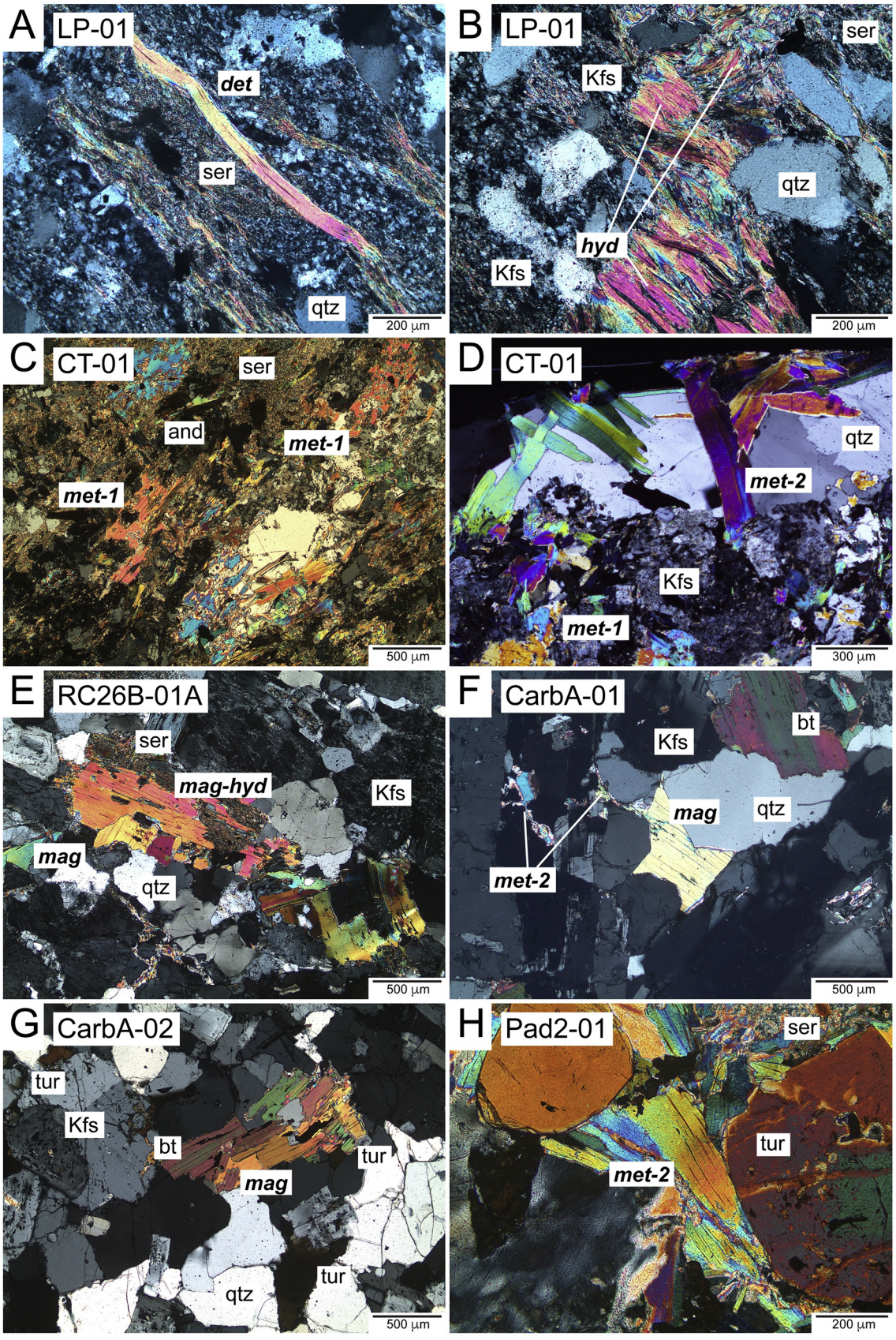


**Fig. 3.** Photomicrographs of representative white mica populations from quartz-arenite LP-01 in the UR (A–B), metamorphically overprinted micaschist CT-01 from the LR (D–E), from granite RC26B-01A (E) and granite CarbA-01 (F), -02 (G), and from the HT vein Pad2-01 (H). All images are taken with crossed polarised light; mineral abbreviations: wm – white mica, bt – biotite, tur – tourmaline, and – andalusite, ser - sericite. See text for further explanations.

populations in CT-01. The first one is medium-grained, sub- to euhedral and occurs in a cross-cutting hydrothermal quartz veinlet (met-2) at the contact towards the host micaschist (Fig. 3D). The second one occurs as sub- to anhedral grains in sericite-rich zones and as alteration on the metamorphic white mica population, and shows μm-scale, cleavage-parallel, oriented intergrowth with biotite, chlorite and exsolution of a sub-μm Fe-Ti oxide phase (Electronic Appendix Fig. A1E). The final population is a margarite-rich white mica that forms < 5 μm-thick reaction fringes between andalusite and the cleavage-parallel intergrown white mica (Electronic Appendix Fig. A1F).

With reference to the alternative petrogenesis of these metamorphic complexes by Carella et al. (2000) and Musumeci et al. (2002) outlined above, it is important to clarify that our samples from the Micaschist and Gneiss Complexes were subjected to contact metamorphism and that two different populations of white mica were recognized: early met-1 metamorphic mica, which may have eventually recrystallized during the contact metamorphic stage; and later met-2 white mica related to contact metamorphism or the early hydrothermal phase.

### 3.3. Granite and high-temperature vein samples

Granite samples from the Radicondoli area (Fig. 1A; RC26B and RC29) in the eastern part of the LTGF have a typical igneous texture – mostly medium- to coarse-grained, subhedral and inequigranular to porphyritic. The major minerals are quartz, K-feldspar, plagioclase, biotite and white mica (5 mod.%), whereas cordierite and andalusite appear as minor minerals. Tourmaline occurs in medium-grained, poikilitic crystals associated with fine-grained chlorite mostly formed by alteration of biotite and white mica. Three populations of white mica are distinguished based on their texture: (1) primary magmatic white mica (hereafter “mag”), that is variably altered to mixtures of sericite and chlorite (Fig. 3E); (2) hydrothermal white mica (hereafter “mag-hyd”) that occurs as finer-grained overgrowth on primary white mica, as fracture-filling, and sub- to anhedral, polycrystalline, pseudomorphic replacement of andalusite (RC26B-02E); and (3) late stage sericite.

Granite samples from the western part of the LTGF come from the Carboli Cbis well (CarbA-01 and CarbA-02; Fig. 1). They have a similar texture, as well as major and minor mineral contents to those of the Radicondoli samples, but lack andalusite. Three white mica populations can be texturally distinguished: a primary magmatic one (mag) with large, sub- to euhedral, single crystals (Fig. 3F–G); an early polycrystalline, likely hydrothermal white mica associated with biotite and tourmaline (met-2, Fig. 3F); and the late hydrothermal sericite. Villa et al. (1997), Carella et al. (2000) and Cavarretta and Puxeddu (2001) present additional petrographic description of granite samples from the LTGF.

We also sampled a HT hydrothermal quartz vein cross-cutting a contact metamorphic phyllite from the Padule 2 well (Pad2-01; see also Gianelli and Ruggieri, 2002). The inequigranular to porphyroclastic texture of the vein consists of quartz, plagioclase and K-feldspar as major minerals and sub- to euhedral tourmaline, biotite and white mica as minor phases. The primary, HT hydrothermal white mica (met-2) is often associated with andalusite and tourmaline, whereas the secondary, LT sericite alters all major mineral phases except quartz and is often intergrown with chlorite (Fig. 3H).

The two additional granite samples are from Porto Azzurro, Elba (CR-1 and -2). White mica is marginally less abundant (1–2 mod.%) than in the granite samples from Larderello, mostly fine-grained and often variably replaced by chlorite. Texturally three white mica populations are recognized: (1) primary, fine-grained, likely magmatic (mag) white mica that is mostly present as pseudo-inclusions in quartz; (2) hydrothermal (mag-hyd), often acicular, spherulitic white mica and (3) late sericite that is quite extensive in sample CR-2. Part of CR-2 is strongly altered and shows a pinkish, brown colour in hand specimen. In this part of CR-2 only minor remnants of the hydrothermal white mica population (mag-hyd) remain, whereas most is replaced by late sericite.

## 4. Analytical methods

### 4.1. Electron-probe micro analysis (EPMA)

Major and minor elements (Si, Ti, Al, Fe, Mg, Ca, Na, K) were quantified with a Jeol-8200 electron microprobe at the Institute of Geological Sciences, University of Bern, Switzerland. Point analyses were placed next to the SIMS spots and acquired with operating conditions of 15 keV, 10 nA and a beam size of 5 μm. Natural mineral standards were used for calibration. The relative standard deviation (RSD %) for the analytes in the natural mineral standards (based on raw counts) is between 0.12% for Mg and 0.3% for Fe. We also acquired compositional X-ray maps for selected, texturally and chemically complex white mica grains with conditions of 15 keV, 100 nA and a dwell time of 200 ms. We used the XMapTools 2.6.1 software (Lanari et al., 2014) to process the raw data, transform the X-ray maps into oxide weight percentages and display the final maps.

### 4.2. Secondary Ion Mass Spectrometry (SIMS)

Oxygen isotope ratios ($^{18}O/^{16}O$) were measured using the Cameca IMS 1280HR instrument at the SwissSIMS laboratory at the University of Lausanne, Switzerland. Between 10 and 105 spot analyses, mostly as multiple spot transects, were made on several discrete grains in each sample. The analytical protocol follows Kita et al. (2009). The SIMS was operated with a 10 kV $Cs^+$ primary beam and a ca. 2 nA current, which resulted in a typical spot size of ca. 15 μm. Charge compensation on the sample was achieved by a vertical incident electron gun. $^{16}O$ and $^{18}O$ secondary ions were accelerated by 10 kV and analysed at a mass resolution (M/ΔM) of 2460 on 2 Faraday cups in multi-collection mode. A transfer magnification of 80 achieved a typical secondary beam intensity of 1.5 to 2.0 × $10^9$ cps for $^{16}O$. Each analysis took ca. 4 min., including pre-sputtering (30 s) and automated centring of the secondary ion peaks. Counts were accumulated during 20 cycles of 5 s for each analysis. The internal error (as 2 × standard error; $2\sigma_m$), also called internal reproducibility, and corresponding to the standard error of the mean during an individual analysis, was between 0.2 and 0.3‰ ($2\sigma_m$). To monitor the instrument stability, three unknown analyses were bracketed by one analysis of the reference material (in-house white mica standard WM-3). In case an instrument drift occurred, it was corrected by applying a first or second order polynomial regression to fit the reference material analyses. A SIMS study by Luisier (2018, unpublished PhD thesis) found no compositional matrix effect in O isotope analysis of four chemically variable white mica samples (WM-1 FeO and MgO of 1.1 and 0.8 wt%; WM-2 FeO and MgO of 2.9 and 4 wt %; WM-3 FeO and MgO of 3.7 and 1.5 wt%; WM-4 FeO and MgO of 1.7 and 3.8 wt%; Electronic Appendix Fig. A2). Bulk laser fluorination analyses on several aliquots of each of the four white mica standards was performed at the Stable Isotope Laboratory of the University of Lausanne using a $CO_2$-laser connected to a Finnigan MAT 253 mass spectrometer (e.g., Lacroix and Vennemann, 2015). During SIMS analysis, instrumental mass fractionation (IMF) correction was based on the in-house standard WM-3 ($\delta^{18}O_{VSMOW}$ = 7.91 ± 0.18‰ 2σ, n = 4; bulk laser fluorination) due to the compositional similarity with the sample white mica and its high $\delta^{18}O$ homogeneity. The IMF is session dependent and the corrected average SIMS $\delta^{18}O$ value for WM-3 is 7.90‰ (2σ; average 0.24, n = 280) (Electronic Appendix Table A1). WM-2 was measured in one session with a corrected average SIMS $\delta^{18}O$ value of 5.64‰ (2σ; average 0.25, n = 26) (Electronic Appendix Table A1). The spot-to-spot, external reproducibility of the unknowns propagated from the repeat measurements of the in-house (WM-3) standard for an individual session, the internal error of the unknown and the standard deviation for the reference value of all the corrected bulk laser fluorination measurements for WM-3, is 0.23–0.51‰ (2σ; average

0.32, n = 405). Individual spots on standard and unknown were afterwards imaged with the SEM to ensure that proper spot placement on a clean sample surface free of mineral inclusions was achieved.

The other white mica in-house standards have accepted $\delta^{18}O_{VSMOW}$ (bulk laser fluorination) values of 10.37 ± 0.12‰ 2σ (WM-1; *n* = 5), 5.64 ± 0.08‰ 2σ (WM-2; n = 4), and 5.32 ± 0.34‰ 2σ (WM-4, n = 4) (Luisier, 2018, unpublished PhD thesis).

### 4.3. Laser Ablation ICP-MS

Trace element concentrations (Li, B, Sc, Ti, V, Rb, Sr, Ba, Pb) were determined for selected samples using an Australian Scientific Instruments (ASI) RESOlution 193 nm laser ablation system coupled to an Agilent 7900 quadrupole mass spectrometer at the Institute of Geological Sciences, University of Bern, Switzerland. Data acquisition was performed in sets of four unknowns bracketed by primary calibration standard NIST 610 and additionally NIST 612 and BIR-1G to monitor data quality and accuracy. The laser spot size was 50 µm in diameter. A laser energy of ca. 8 mJ resulted in a sample fluency of ca. 3 J/cm$^2$ applied at a repetition rate of 5 Hz. Each analysis was 90 s with 30 s ablation. The following isotopes were measured: $^{7}$Li, $^{11}$B, $^{29}$Si, $^{45}$Sc, $^{49}$Ti, $^{51}$V, $^{85}$Rb, $^{88}$Sr, $^{138}$Ba, and $^{208}$Pb. We used $^{29}$Si for internal standardization, based on EPMA measurements of the $SiO_2$ concentration in each sample white mica. Data reduction was performed offline with Iolite (Paton et al., 2011), and detection limits were calculated with the formulation detailed in Pettke et al. (2012). Repeatability based on measurements of NIST 612 and BIR-1G is 3% or better for most elements, except B and Rb with 10% and 6%, respectively. All analytes

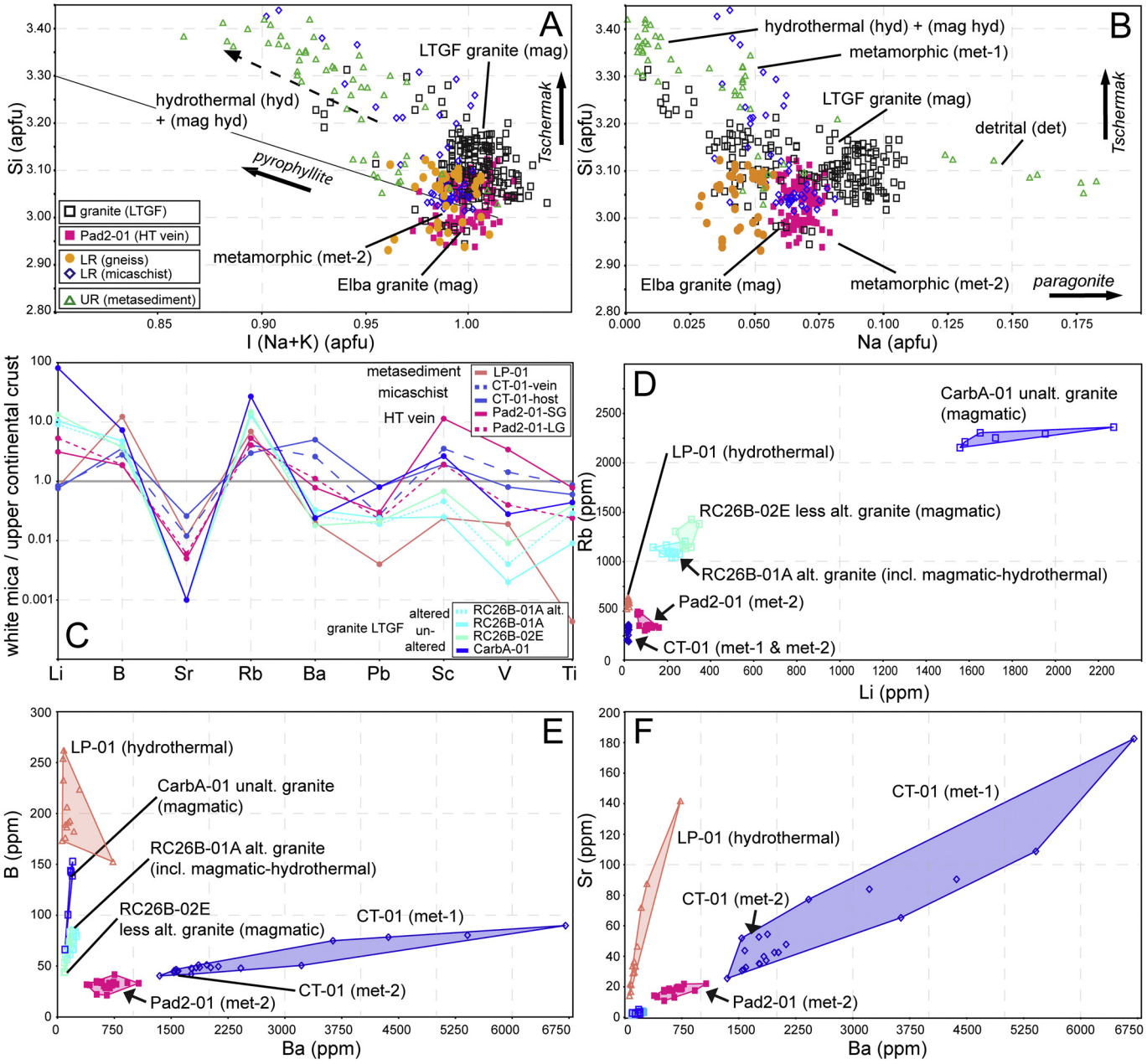


**Fig. 4.** A and B – chemical data for white mica from the LTGF in atoms per formula unit (apfu) with major cation exchange vectors (A – pyrophyllite and Tschermak; B – paragonite and Tschermak). Samples have been grouped according to lithology and position in the LTGF – Upper Reservoir (UR) and Lower Reservoir (LR); Shaded areas indicate approximate compositions of distinct white mica populations with common overlap; the dashed arrow shows a general trend of hydrothermal white mica; C – Trace element data for selected samples normalized on upper continental crust with values from Wedepohl (1995) and Rudnick and Gao (2004); In the key, Pad2-01-LG and Pad 2-01-SG indicate large and small grain sizes, respectively. D to F – Trace element plots for selected samples.

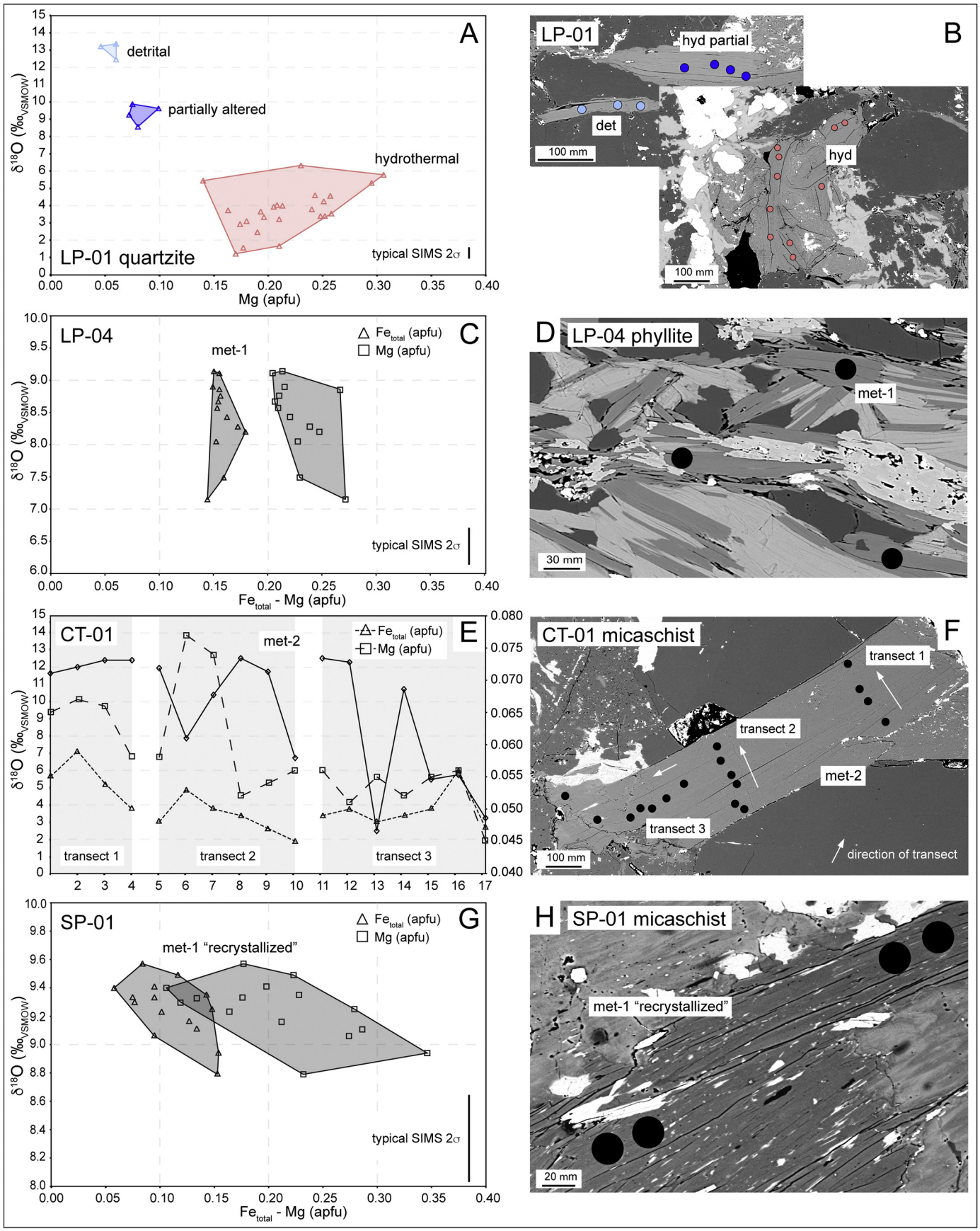


**Fig. 5.** Microscale $\delta^{18}O$ variability of white mica versus chemistry and texture. A–B – texturally variably white mica in metasedimentary sample LP-01; C–D – met-1 white mica in phyllite LP-04 intergrown with chlorite and epidote; E–F – HT vein white mica met-2 in contact metamorphic sample CT-01; G–H – recrystallized met-1 in contact metamorphic sample SP-01. Circles on BSE images depict the location and size of the SIMS analyses.

were above detection limits. Detection limits were around 0.1 ppm or lower for all elements, except B with ca. 0.5 ppm.

### 4.4. $^{39}Ar$-$^{40}Ar$ dating

Analyses were performed on a NuInstrument™ Noblesse™ multi-collector noble gas mass spectrometer following the procedures of Montemagni et al. (2018). Special care was placed on avoiding Cd shielding, as the information provided by the Cl/K ratio is of decisive importance in unravelling the various white mica generations present in most samples. Samples ranging between 2 and 8 mg were separated by hand-picking after gently hand-crushing the small (few hundreds of mg) rock chips from selected well samples. Stoichiometry of the hand-picked white mica was monitored from the total $^{39}Ar$ production.

## 5. Results

### 5.1. White mica chemistry

We analysed major and minor elements next to SIMS analytical spots in white mica from 13 samples, and a selection of trace elements in white mica from six samples (Electronic Appendix Tables A2–A3; Fig. 4). Although the composition of the total sample population is variable, the majority of the analysed white mica can be classified as

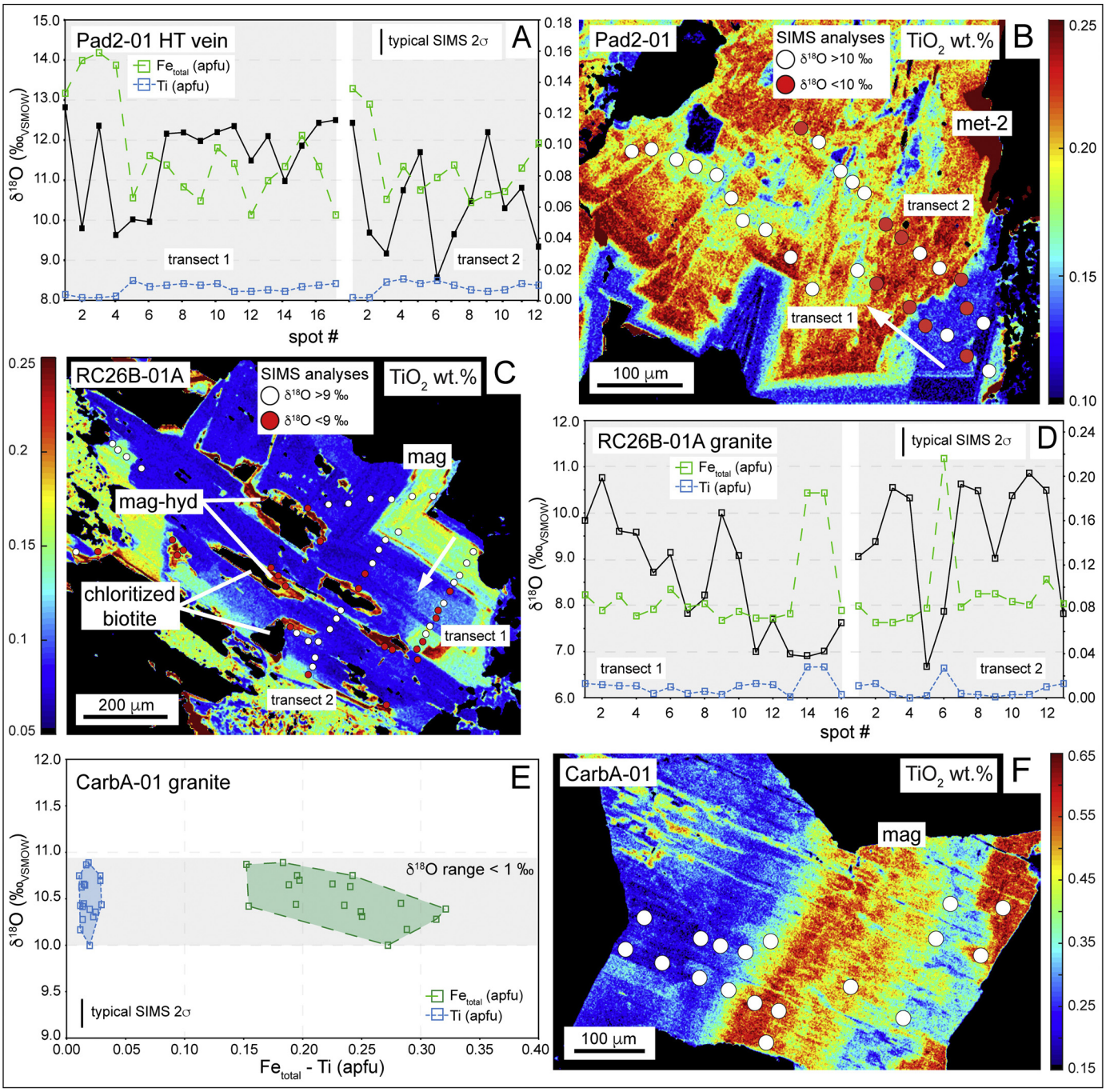


**Fig. 6.** Microscale $\delta^{18}O$ variability of white mica versus chemistry and texture. A–B – chemically variably white mica met-2 in HT vein sample Pad2-01; C–D – primary granitic white mica with included chloritized biotite surrounded by altered areas in sample RC26B-01A; E–F – primary granitic white mica in sample CarbA-01. EPMA elemental maps in B, C, F depict zonation in $TiO_2$ (wt%). Spots on EPMA maps depict the location of the SIMS analyses.

muscovite based on Rieder et al. (1998) (K: 0.93 ± 0.03, 1σ, n = 405, Si: 3.1 ± 0.1, $^{VI}$Al: 1.8 ± 0.1; atoms per formula unit – apfu, per 11 oxygens). The compositional variability is the result of three dominant cation exchanges (Fig. 4A–B), 1) paragonite-muscovite [K-Na], 2) Tschermak [$Si^{4+}(Mg^{2+}, Fe^{2+})$—$2Al^{3+}$] and 3) pyrophyllite [$(K, Na)^{1+}Al^{3+}$—$\square_1Si^{4+}$]. Granite and contact metamorphic lithologies contain white mica with similar composition, whereas metasedimentary white mica shows the highest variability via exchange 1 and 3 (Fig. 4A–B). The white mica trace element composition (metasediment, micaschist – HT vein, granite) shows broadly similar trends regardless of protolith (Fig. 4C). The incompatible elements Sc, V, and Ti, as well as the mobile elements Sr and Ba (Fig. 4F) are more abundant in the micaschist and HT vein (CT-01 and Pad2-01) than in the granite and metasediment samples (RC26B, CarbA and LP-01). Lithium, however, is much more abundant in the granitic white mica and up to a hundred times enriched with respect to average upper continental crust (from Wedepohl, 1995, Rudnick and Gao, 2004; Fig. 4C–D). All samples are also variably enriched in B (< 12× in metasediment LP-01; Fig. 4C) and Rb (< 27× in granite CarbA-01) (Fig. 4C–F) with respect to upper continental crust values.

White mica from the metasedimentary samples (LP-01, LP-04, MV2A-01) shows inter-grain compositional features reflecting the different texture. The detrital population (det) in LP-01 and MV2-01 has low $Fe_{tot}$ + Mg of ≤0.17 apfu and high Na of 0.06 to 0.15 apfu. The metamorphic population (met-1) in LP-04 has high $Fe_{tot}$ + Mg of ≤0.38 apfu, and the late hydrothermal population (hyd) in LP-01 has a distinctively low Na of ≤0.01, high Mg of ≤0.22 but low $Fe_{tot}$ of 0.04 apfu (Electronic Appendix Table A2; Figs. 4, 5A). Although the white mica populations in the gneiss samples VC11 (met-1 and -2) have partly overlapping composition in the Si-I (interlayer cations; Na and K) space (Electronic Appendix Table A2; Fig. 4A–B) their Fe and Mg concentrations are very different. The vein white mica met-2, has much lower $Fe_{tot}$ and Mg concentrations than the host white mica met-1 (0.08 versus 0.18 and 0.009 versus 0.14 apfu, respectively; Electronic Appendix Fig. A3 and Table A1).

The composition of white mica in the contact metamorphic micaschist (CT-01 and SP-01) and the HT vein (Pad2–01) on the other hand is not related to their textures (met-1 or met-2, Figs. 4–6 ). For instance, a small (ca. 100 µm) met-1 grain in CT-01 has high Si (≥3.2 instead of ≤3.05 apfu) and low Na (< 0.05 apfu). Intra-grain variations in Fe-Mg-Ti occur in large white mica (met-2) in Pad2-01 (HT vein) and CT-01. In the latter the variations are most pronounced in Mg (from 0.045 to 0.077 apfu) and to a lesser degree in $Fe_{tot}$ (Fig. 5E–F). In Pad2-01, a ≤ 100 µm rim has higher Fe and Mg (both from ca. 0.06 to ca. 0.15 apfu), and lower Ti (from 0.013 to 0.002 apfu) with respect to the rest of the grain (Fig. 6A–B).

Granite from Radicondoli (RC26B and RC29) and the altered granite from Elba (CR-2) contain magmatic white mica (mag) with a low Tschermak component ($Fe_{tot}$ + Mg = 0.16–0.27 apfu), close to the true muscovite composition as defined in Guidotti (1984) (Electronic Appendix Fig. A3). White mica from the Carboli granite (CarbA; mag), some altered white mica domains in RC26B (mag-hyd), and the unaltered sample from Elba (CR-1) extend towards the ferriphengite and ferrimuscovite compositions ($Fe_{tot}$ + Mg = 0.39–0.40 apfu; Electronic Appendix Fig. A3). However, both “mag and mag-hyd” white mica populations from the LTGF show irregular Fe-Mg-Ti zonation with variations in $Fe_{tot}$ + Mg of 0.3–0.5 apfu and in Ti of 0.004–0.03 apfu (Electronic Appendix Table A2; Fig. 6C–F). The white mica in the Elba granite shows inter-sample variations. Primary white mica in CR-1 is on average higher in $Fe_{tot}$ and Mg (0.19 and 0.2 apfu) than primary white mica in CR-2 (0.07 and 0.04 apfu). However, there is a perceptible Mg increase from primary to secondary white mica in CR-2 with 0.04 and 0.11 apfu, respectively (Table 2; Fig. 7D).

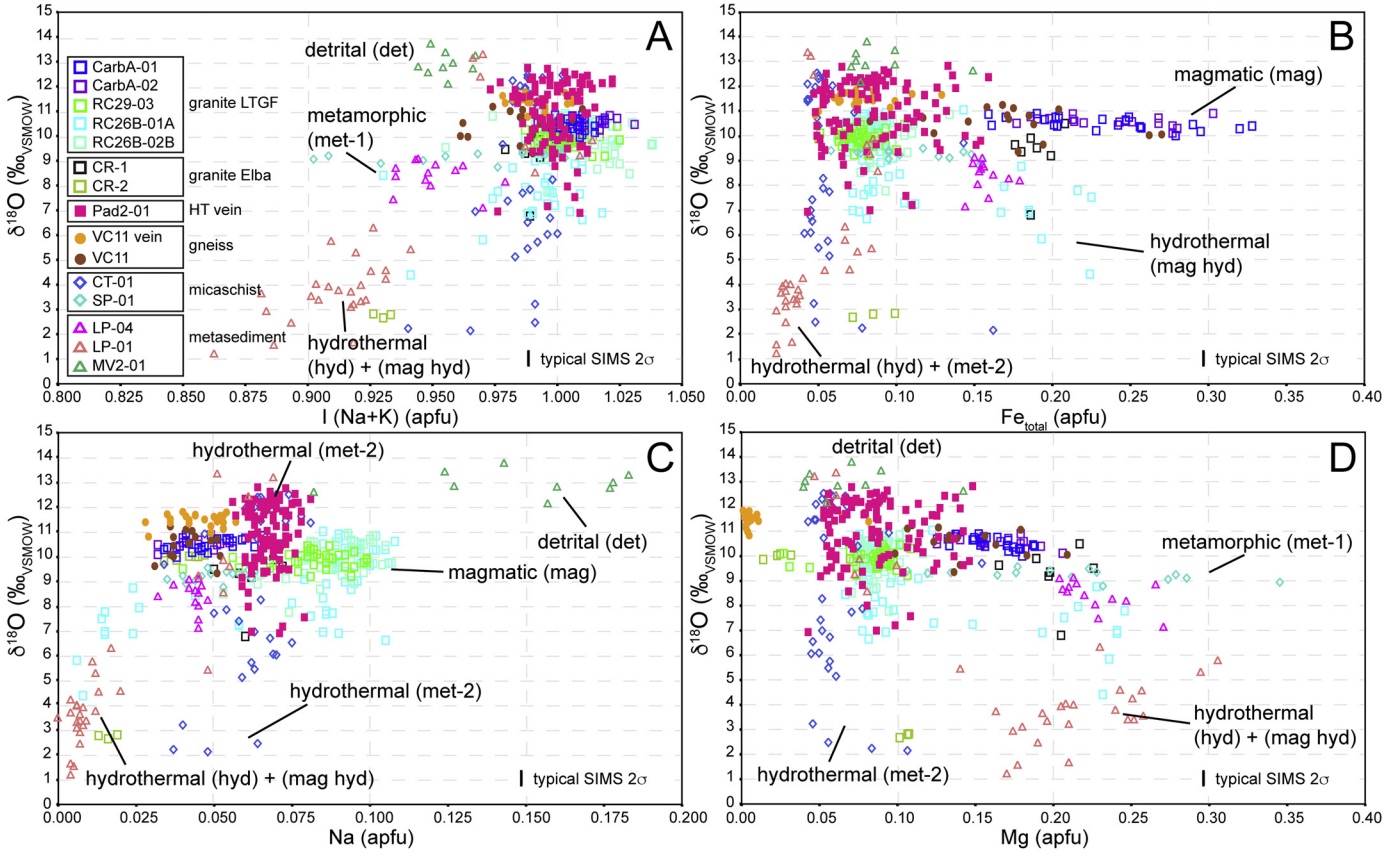


**Fig. 7.** SIMS $\delta^{18}O$ data for white micas from the LTGF versus mineral composition. Distinct white mica populations are labelled, however overlap occurs.

**Table 2**
SIMS $\delta^{18}O$ data (per mil VSMOW) of white mica and fluid in equilibrium at representative temperatures.

| Sample | | LP-01* | | | LP-04 | MV2A-01 | VC11–01-2a | VC11–01-19b | SP-01 | CT-01* | | Pad2–01* | CarbA-01 | CarbA-02 | RC29–03 | RC26B-01A* | | RC26B-02E | CR-1 | CR-2 | |
|---|---|---|---|---|---|---|---|---|---|---|---|---|---|---|---|---|---|---|---|---|---|
| Population | | det | hyd partial | hyd | met-1 | det | met-1 | met-2 | met-1 | met-1 | met-2* | met-2 | mag | mag | mag | mag | mag-hyd | mag | mag | mag | hyd |
| n analyses | T°C | 3 | 4 | 24 | 13 | 9 | 16 | 23 | 15 | 19 | 26 | 102 | 21 | 18 | 37 | 31 | 21 | 42 | 7 | 7 | 5 |
| M $\delta^{18}O$ (‰) | | 13.2 | 9.5 | 3.7 | 8.6 | 12.9 | 10.6 | 11.5 | 9.3 | 11.3 | 10.6 | 11.1 | 10.4 | 10.6 | 9.9 | 10.0 | 7.7 | 9.9 | 9.5 | 10.0 | 2.8 |
| $\bar{x}$ $\delta^{18}O$ (‰) | | 13.0 | 9.3 | 3.7 | 8.4 | 13.0 | 10.5 | 11.5 | 9.2 | 9.6 | 9.4 | 10.9 | 10.5 | 10.6 | 9.9 | 10.0 | 7.5 | 10.0 | 9.3 | 10.0 | 2.9 |
| 1σ | | 0.5 | 0.6 | 1.3 | 0.6 | 0.5 | 0.6 | 0.3 | 0.2 | 3.3 | 3.1 | 1.3 | 0.2 | 0.2 | 0.3 | 0.6 | 1.0 | 0.6 | 1.2 | 0.1 | 0.3 |
| Min. | | 12.5 | 8.6 | 1.2 | 7.2 | 12.1 | 9.4 | 10.8 | 8.8 | 2.2 | 2.5 | 6.9 | 10.0 | 10.1 | 9.2 | 9.0 | 4.4 | 8.5 | 6.8 | 9.9 | 2.7 |
| Max. | | 13.4 | 9.9 | 6.3 | 9.1 | 13.8 | 11.2 | 11.8 | 9.6 | 12.4 | 12.5 | 12.8 | 10.9 | 10.9 | 10.5 | 11.0 | 8.8 | 11.0 | 10.5 | 10.1 | 3.4 |
| *T°C (in-hole)*** | | 180 | 180 | 180 | 300 | 265 | 340 | 340 | 440 | 320 | 320 | 340 | 400 | 400 | 400 | 350 | 350 | 350 | | | |
| Calculated $\delta^{18}O$ (‰) of fluid in oxygen isotope equilibrium with white mica at T°C (after Zheng, 1993) | | | | | | | | | | | | | | | | | | | | | |
| Min. | 150 | 5.2 | 1.3 | −5.9 | – | – | – | – | – | – | – | – | – | – | – | – | – | – | −0.4 | 2.6 | −4.5 |
| Max. | | 6.2 | 2.7 | −0.8 | – | – | – | – | – | – | – | – | – | – | – | – | – | – | 3.3 | 2.9 | −3.8 |
| Min. | 200 | 7.9 | 4.0 | −3.2 | 2.6 | 7.7 | – | – | – | – | – | – | – | – | – | – | – | – | 2.3 | 5.3 | −1.8 |
| Max. | | 8.9 | 5.4 | 1.8 | 4.6 | 9.3 | – | – | – | – | – | – | – | – | – | – | – | – | 6.0 | 5.6 | −1.1 |
| Min. | 300 | 11.0 | 7.0 | −0.2 | 5.7 | 10.7 | 7.9 | 9.4 | 7.3 | 0.7 | 1.0 | 5.5 | – | – | – | 7.5 | 2.9 | 7.1 | 5.3 | 8.4 | 1.2 |
| Max. | | 12.0 | 8.4 | 4.9 | 7.7 | 12.3 | 9.8 | 10.4 | 8.2 | 10.9 | 11.1 | 11.3 | – | – | – | 9.6 | 7.3 | 9.5 | 9.0 | 8.7 | 1.9 |
| Min. | 400 | – | – | – | 7.2 | 12.2 | 9.4 | 10.8 | 8.8 | 2.2 | 2.5 | 6.9 | 10.0 | 10.1 | 9.2 | 9.0 | 4.4 | 8.5 | – | – | – |
| Max. | | – | – | – | 9.1 | 13.8 | 11.2 | 11.8 | 9.7 | 12.4 | 12.5 | 12.8 | 10.9 | 10.9 | 10.5 | 11.0 | 8.8 | 11.0 | – | – | – |
| Min. | 500 | – | – | – | – | – | 10.1 | 11.6 | 9.5 | 2.9 | 3.2 | 7.7 | 13.9 | 10.7 | 10.0 | 9.8 | 5.1 | 9.3 | – | – | – |
| Max. | | – | – | – | – | – | 12.0 | 12.6 | 10.4 | 13.1 | 13.3 | 13.6 | 14.8 | 11.6 | 11.2 | 11.8 | 9.5 | 11.7 | – | – | – |
| Min. | 600 | – | – | – | – | – | 10.4 | 11.9 | 9.9 | 3.2 | 3.6 | 8.0 | 12.6 | 11.1 | 10.3 | 10.1 | 5.5 | 9.6 | – | – | – |
| Max. | | – | – | – | | – | 12.3 | 12.9 | 10.8 | 13.5 | 13.6 | 13.9 | 13.5 | 12.0 | 11.5 | 12.1 | 9.9 | 12.1 | – | – | – |
| Δmin - max | | 1.0 | 1.4 | 5.1 | 2.0 | 1.7 | 1.9 | 1.0 | 0.9 | 10.3 | 10.1 | 5.9 | 0.9 | 0.8 | 1.2 | 2.0 | 4.4 | 2.4 | 3.7 | 0.3 | 0.7 |

$\delta^{18}O$ values are given as median (M) and average ($\bar{x}$) of each white mica population with 1σ standard deviation and minimum and maximum; fluid compositions are calculated for T°C range most likely experienced by sample * samples used for $^{39}Ar$-$^{40}Ar$ dating **p.d.T. literature data from same well and depth (or extrapolated at the depth from mean geothermal gradient of LTGF) or close vertical proximity from Cavarretta et al., 1980; Batini et al., 1985; Petrucci et al., 1994; Carella et al., 2000; Ruggieri and Bertini, 2000; Gianelli and Laurenzi, 2001; Gianelli et al., 2001; Villa et al., 2001; Boiron et al., 2007.

### 5.2. White mica $\delta^{18}O$ data

In-situ microanalyses of white mica identified a considerable spread of $\delta^{18}O$ values between 2 and 12‰ on grain scale and 1–14‰ on sample scale (Table 2; Figs. 5–7). Texturally and chemically distinct white mica populations (Figs. 5, 7) from the metasediment samples (LP-01, LP-04, MV2–01) from the UR display this large spread in $\delta^{18}O$, ranging from late hydrothermal (hyd) mica with $\delta^{18}O$ of 1–6‰, over the partially altered mica population (hyd partial, $\delta^{18}O$ = 8–9‰) to the detrital mica (det, $\delta^{18}O$ = 14‰) (Fig. 5A–B). Metamorphic white micas met-1 in sample LP-04 have homogeneous $\delta^{18}O$ values averaging 8.4 ± 0.6‰ 1σ, similar to the $\delta^{18}O$ values of partially altered white mica in LP-01 (Fig. 5A–D; Table 2).

Downhole within the LR, white micas from the two contact metamorphic micaschist samples CT-01 and SP-01 show different signatures. Sample SP-01 has homogeneous white mica with a $\delta^{18}O$ value of 9.2 ± 0.2‰, 1σ (met-1; Fig. 5G–H). In sample CT-01, white micas of variable texture and chemistry (met-1, -2, Fig. 5E–F) record a large spread in $\delta^{18}O$ from 2 to 12‰. Both the hydrothermal veinlet white mica met-2 and the host rock metamorphic met-1 in micaschist CT-01 have the same spread in $\delta^{18}O$ values (Fig. 7). Cleavage-parallel and -perpendicular transects in a large grain of met-2 display the largest measured intra-grain $\delta^{18}O$ variation of almost 10‰ (Fig. 5E–F). The $\delta^{18}O$ values of HT hydrothermal vein white mica (met-2) from sample Pad2-01 also partly overlap with this range and show an inter-grain spread of ca. 6‰ (from 6.9 to 12.8‰; Table 2) and a less pronounced, intra-grain variability of up to 4‰ on spots < 100 µm apart (Fig. 6A–B). In the gneiss samples from VC11 the two white mica populations (met-1, -2) display a small but consistent difference in $\delta^{18}O$. The host white mica met-1 has an average $\delta^{18}O$ value of 10.5 ± 0.6‰ 1σ and the vein white mica met-2 an average of 11.5 ± 0.3‰ 1σ (Table 2).

In the two granite samples from Carboli (CarbA-01, -02) grains of mag and met-2 white mica were analysed. Although texturally different, both populations vary similarly in composition on intra-grain scale (e.g. Mg and $Fe_{tot}$) but have very homogeneous primary magmatic $\delta^{18}O$ values of 10.5 ± 0.2‰ (n = 21) in CarbA-01 and 10.6 ± 0.2‰ 1σ (n = 18) in CarbA-02 (Figs. 6–7). White micas from the two older granite samples from Radicondoli (RC26B-01A, -02B) have $\delta^{18}O$ values ranging from 4.5 to 11‰. The intra-grain $\delta^{18}O$ variability of up to 6‰ in primary magmatic white mica in RC26B-01A occurs generally in domains with higher Fe and Mg (mag-hyd) around inclusions of completely chloritized biotite (Fig. 6C–D). For grains with similar, but barely altered domains, where biotite is still present (RC26B-02E), the intra-grain $\delta^{18}O$ variability is reduced to ≤2‰ (Table 2). The background $\delta^{18}O$ value for the clearly magmatic white mica (mag) grains is 10 ± 1‰ (Figs. 6–7). The granite samples from Porto Azzurro, Elba (CR-1, -2) show similar $\delta^{18}O$ values in white mica (mag) from the unaltered samples with averages of 9.3 ± 1.2 and 10 ± 0.1‰, respectively (Fig. 7; Table 2). The strongly altered part of sample CR-2, however, contains an altered grain (mag-hyd) with a low average $\delta^{18}O$ of 2.9 ± 0.3‰ (Fig. 7; Table 2). The alteration front effectively divides the thin section in two halves and the variation in $\delta^{18}O$ of ca. 7‰ occurs over a distance of ca. 5 mm.

In summary, white mica with homogeneous $\delta^{18}O$ values is found in the metasedimentary samples as detrital grains (det) and partially overprinted grains (hyd partial) (Fig. 8). Contact metamorphic micaschist SP-01 also contains white mica with homogeneous $\delta^{18}O$ values (met-1). All unaltered granite white mica (mag) are within uncertainty ($\delta^{18}O$ of 10.0 ± 0.6‰), with the exception of the altered population (mag-hyd) with $\delta^{18}O$ values as low as 2.7‰ in CR-2 (Figs. 7 and 8). The largest $\delta^{18}O$ variations of up to 10‰ are found in the secondary, hydrothermal white mica (hyd) and the HT vein white mica (met-2). In most cases intra-grain $\delta^{18}O$ variations are unrelated to chemical variations in major and trace elements, but two notable exceptions occur: (1) the altered, granitic white mica (mag-hyd) and (2) the metasedimentary hydrothermal white mica (hyd). For both, the $\delta^{18}O$ decrease is accompanied by an increase in either Fe, Mg, Ti, or only Mg, coupled with a decrease in Na (Fig. 7C–D).

### 5.3. White mica $^{39}Ar$-$^{40}Ar$ data

The ages estimated from the $^{39}Ar$-$^{40}Ar$ analyses (Electronic Appendix Table A4) and their absolute errors are summarized in

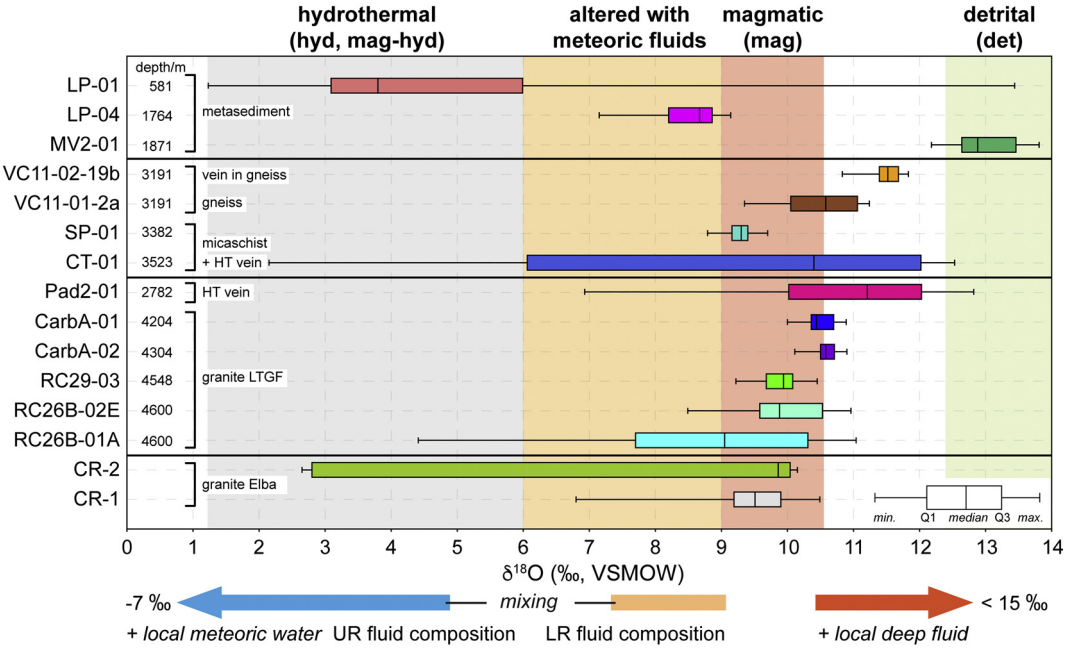


**Fig. 8.** Box and whisker plot of SIMS $\delta^{18}O$ data for white mica from the LTGF from the UR to the LR and the sampled granite from Elba at the bottom. Different white mica populations are marked in shaded boxes (see text for discussion). The line in the individual boxes denotes the median of the specific sample, the left and right of the box are the lower (25th percentile) and upper (75th percentile), respectively and the whiskers show the minimum and maximum values. Sources for the LTGF fluid compositions are given in Fig. 2.

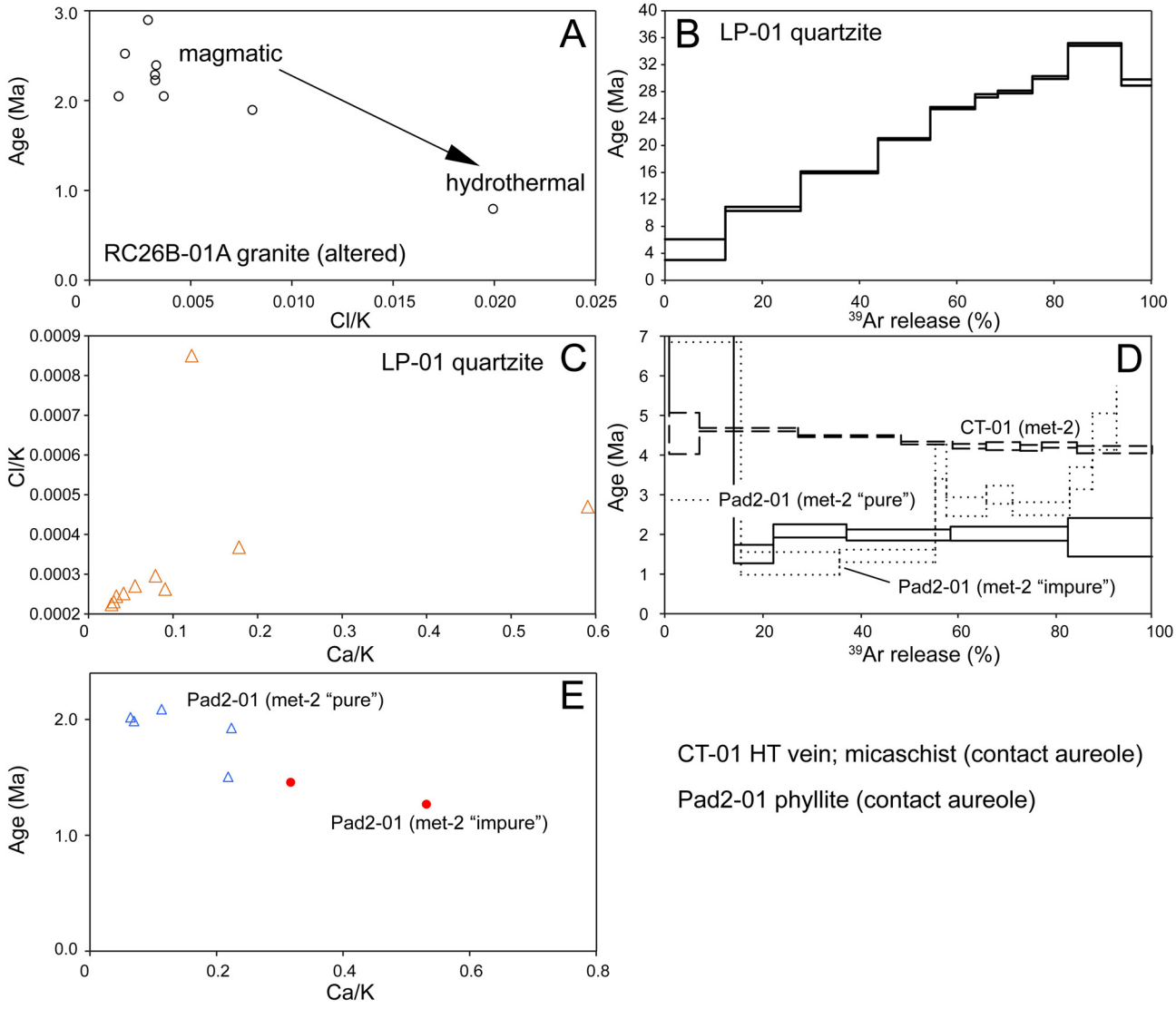


**Fig. 9.** $^{39}Ar$-$^{40}Ar$ results. A – Cl/K – age common-denominator three-isotope correlation diagram for white mica RC26B-01A. Cl/K is calculated as ($^{38}Ar_{Cl}/^{39}Ar_K$)*0.178; Ca/K is calculated as ($^{37}Ar_{Ca}/^{39}Ar_K$)*1.94; the age is calculated as (1/λ)*ln(1 + J*$^{40}Ar^*/^{39}Ar_K$) (whereby the J parameter reflects the irradiation intensity), which simplifies to ($^{40}Ar/^{39}Ar_K$)*1.48 for the present ages < 10 Ma. B–C – Age spectrum and Ca/K-Cl/K common-denominator three-isotope correlation diagram for white mica LP-01. The staircase-shaped spectrum is a tell-tale sign of a phase mixture (Villa and Hanchar, 2017). D – Age spectra of metamorphic white mica from two neighbouring wells. Dashed line plateauing off at 4.2 Ma, CT-01. Solid line plateauing at 2.0 Ma, "pure" handpicked white mica from Pad2–01; dotted line, "impure" mica, consisting of initially discarded mica grains from the same crushed rock chip. E – Ca/K-age three-isotope correlation diagram for the "pure" (open triangles) and "impure" (filled circles) Pad2–01 white mica aliquots.

Table 3. A useful reproducibility check is provided by RC26B-01A as a dry aliquot of this sample was reported by Villa et al. (1997). Both dry muscovite aliquots from the RC26B-01A sample reveal the > 2.5 Ma ( ± 0.3 Ma, this work) old magmatic muscovite (mag). The petrographic observation of two generations of hydrothermal muscovite is not clearly reproduced in Fig. 9A. The most plausible explanation is that during hand-picking (as performed both by Villa et al. (1997) and, more extensively, in the present work) the larger, more euhedral, fresher-looking grains were favoured over smaller ones intergrown with impurities, thereby enriching mag > mag-hyd > sericite. Quartzite sample LP-01 contains two mica generations (with admixture of two additional, less abundant components), as shown by the linear array in the Ca/Cl/K diagram: a detrital mica > 40 Ma old and a hydrothermal one ≤4 Ma old (Fig. 9B–C). The thermal decrepitation of fluid inclusions in a quartz separate from the same rock chip has yielded $^{40}Ar/^{36}Ar$ = 299.6 ± 1.0, indicating that the circulating fluid that reacted with LP-01 was not significantly enriched in 'excess Ar'. Age spectra of metamorphic white mica (met-2) from the two neighbouring wells CT-01 and Pad2-01 is shown in Fig. 9D. Sample CT-01 has a plateau age of 4.2 ± 0.02 Ma Ma. The two white mica separates analysed from Pad2-01, (1) a "pure" handpicked white mica and (2) an "impure" white mica, consisting of white mica grains from the same crushed rock chip, show ages of 2.0 ± 0.04 Ma and 1.27 ± 0.14 Ma, respectively. The data show that even the extensively hand-picked "pure" muscovite fractions (in Fig. 9E, open triangles) have a mixing trend towards the "impure" aliquots (filled circles), and thus contain significant amounts of the ≤1.2 Ma generation. The age difference of 2 Ma between met-2 stage white micas from CT-01 and from Pad2-01, which are separated by a map distance of 2 km (Fig. 1A) is robust evidence of spatial heterogeneity in hydrothermal circulation at the km scale over time. The chemical (Electronic Appendix Tables A2–A3) and chronological difference between the "pure" and "impure" mica aliquots within the same sample is robust evidence of spatial heterogeneity in hydrothermal circulation at the mm scale.

## 6. Discussion

### 6.1. Interaction of meteoric fluids with white mica in the Upper Reservoir

Our $\delta^{18}O$ data for white micas are consistent with the accepted LTGF reservoir model discussed above based on bulk rock stable isotope and fluid inclusion data. In samples from the UR the $\delta^{18}O$ values of the detrital white mica (13 ± 0.5‰,1σ; Figs. 5A–B, 8) resemble that of bulk micaschist from the Northern Apennines, as a reference for pristine, unaltered micaschist and likely concur with the > 40 Ma age group (Figs. 2, 9B; Gianelli and Ruggieri, 2002). Combined with their texture and distinct chemistry (Figs. 5A–B, 7) this indicates that they are chemically and isotopically undisturbed by the incursion of surface water with a $\delta^{18}O$ value of −7‰ into the UR. The late hydrothermal white mica, however, has similar $\delta^{18}O$ values (1–6‰) to other secondary minerals and the meteoric-dominated fluid circulating in the late hydrothermal stage (Fig. 2; Petrucci et al., 1994; Boyce et al., 2003). This white mica population that precipitated during the late hydrothermal stage is in equilibrium with Mg-rich, low-Na, low-$\delta^{18}O$ fluids of −4 to 1‰ (at 180 °C p.d.T., fractionation factors from Zheng, 1993; Table 2). This fluid percolated downwards to depths of several hundred meters and was heated to temperatures of 100–250 °C (Fig. 10; Gianelli and Ruggieri, 2002). Geothermal fluids at the LTGF have a high B content (Cavarretta et al., 1980) and during passage through the crust, especially through the carbonate-evaporite reservoir, the fluids likely leached B and precipitated the high-B, hydrothermal white mica in sample LP-01. The late-hydrothermal, low-$\delta^{18}O$ white mica in metasedimentary rocks of the UR has higher B contents than those in micaschists, gneisses and granites of the LR (ca. 200 ppm versus ca. 120 ppm in unaltered granite CarbA-01; Electronic Appendix Table A3) that probably also interacted with Li-B-rich fluids expelled by the crystallizing intrusions (Gianelli and Ruggieri, 2002; Dini et al., 2005; Boiron et al., 2007). However, the presence of tourmaline in the LR, probably buffered the B content of the LR fluids, whereas tourmaline is absent in sample LP-01.

Steam samples from the UR (ca. 1 km b.g.l.) in the temperature range of 100–250 °C have $\delta^{18}O$ values between −6 to 0‰ (Panichi et al., 1974; D'Amore et al., 1987; Petrucci et al., 1994); these values are in agreement with our calculations for the $\delta^{18}O$ values of the hydrothermal fluids in exchange equilibrium with hydrothermal white mica, −4 to 1‰ (Fig. 10). The range of $\delta^{18}O$ values in white mica from the uppermost metasediment sample LP-01 (Figs. 5A, 7, 8) indicates that equilibrium between the different grains was not reached. The micro-scale proximity of ca. 100 µm between detrital and hydrothermal grains (Fig. 5A–B) testifies to very selective fluid infiltration and fluid rock interaction at spatial scales of 100 µm. Since temperature is largely uniform at this scale, variation in the extent of fluid infiltration and accompanying fluid-rock interaction, reflecting small scale variation in local secondary permeability, is the key factor controlling the reactivity and preservation potential of the primary chemical and $^{18}O/^{16}O$ in white mica. Secondary permeability becomes less relevant with depth, especially at the base of the LR or the K-horizon, where the brittle-ductile transition is supposed to occur and at most strain rates fracture opening, and propagation is effectively zero. As such, ambient temperature in the LR, which is up to 300 °C higher that in the UR, is an important factor influencing secondary permeability, whereas in the UR it is not.

We propose that recrystallization is another dominant factor influencing the oxygen isotope retentivity of white mica at the LTGF. The rate of recrystallization, and thus effective stable isotope exchange is increased by fluid flow, higher temperatures and spatial and temporal variations in the surface area of the reacting white mica (e.g. Baumgartner and Valley, 2001). Limited fluid flow, temperatures < 350 °C and variations in micro-fracturing, especially in brittle conditions in the UR (e.g. LP-01) may thus limit the rate of fluid-rock reaction by recrystallization, and hence limit the rate of oxygen isotope exchange. Detrital grains in phyllite MV2-01 that escaped recrystallization, for instance, retained high and homogeneous $\delta^{18}O$ values that are interpreted as primary (Figs. 7, 8), despite the mineralogical evidence for a strong late stage hydrothermal overprint of this sample interval with p.d.T. of ca. 265 °C and past temperature up to 340 °C as indicated by fluid inclusions (Ruggieri et al., 1999). The partially altered/recrystallized white mica grains in LP-01 on the other hand, have a similar $\delta^{18}O$ (ca. 9.3‰), but slightly different chemistry than the met-1 grains in LP-04 (ca. 8.4‰), around 1.2 km deeper in the same well (Fig. 7; Table 2). White mica in LP-04 is associated with abundant chlorite, has Mg contents overlapping with those of hydrothermal white mica (Fig. 7D) and is isotopically homogeneous. This is interpreted as a result of extensive recrystallization under late stage hydrothermal conditions, which homogenized this sample interval. The average white mica $\delta^{18}O$ of ca. 8.4‰ is in equilibrium with quartz of ca. 13‰ in similar phyllite intervals (from the Phyllitic-Quartzitic Complex) measured by Petrucci et al. (1993) in other wells at ca. 300 °C. If taken as equilibrium, as calculations from Petrucci et al. (1993) and in this study indicate, these two minerals define a fluid composition of 6.9‰; (Table 2). This value is in accord with the calculated $\delta^{18}O_{fluid}$ values of 4–8‰ for infiltrating fluids at 2 km depth presented by Petrucci et al. (1993) and D'Amore and Bolognesi (1994) for temperatures between 260 and 360 °C. Since the partially altered grains in LP-01 with similar $\delta^{18}O$ values of ca. 9.3‰ (Fig. 5A–B) occupy a much higher stratigraphic position within the LTGF, their re-equilibration temperature should be lower at ca. 180 °C (D'Amore and

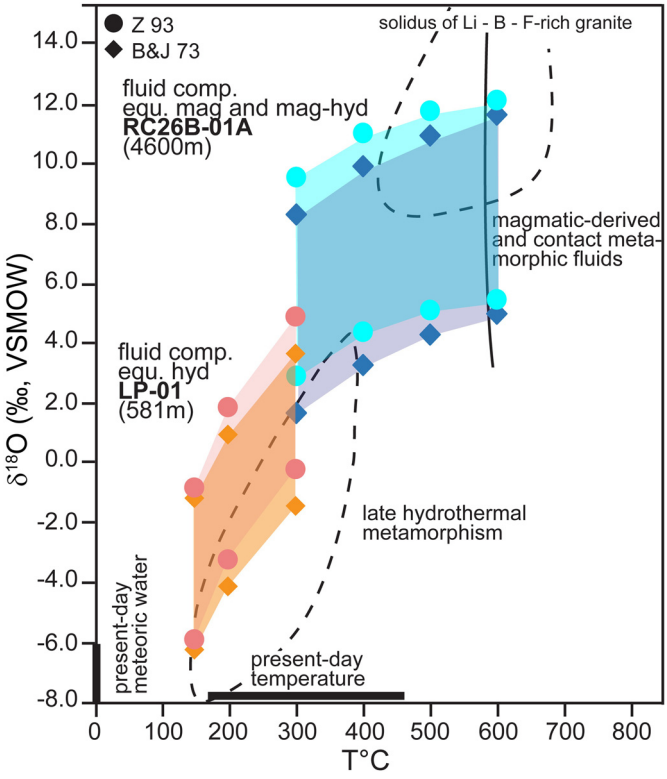


**Fig. 10.** T-X conditions for the two major hydrothermal stages at the LTGF reporting $\delta^{18}O$ of the fluid in equilibrium with the analysed white mica (mineral-fluid fractionation factors from Bottinga and Javoy, 1973 – B&J 73 diamond – and Zheng, 1993 – Z93 circle) at the temperature range proposed by Gianelli and Ruggieri (2002 and ref. therein) for the two stages. The two coloured fields denote data for fluids linked to the initial HT magmatic-dominated stage (RC26B-01A/02E, in turquoise and purple, using two different mica-water fractionation factors) and the LT late meteoric-dominated stage (LP-01, in red and orange using two different mica-water fractionation). (For interpretation of the references to colour in this figure legend, the reader is referred to the web version of this article.)

Bolognesi, 1994). Therefore, the corresponding fluid has a lower $\delta^{18}O$ of ca. 4‰ (Table 2). These values indicate that water-rock interaction, as a function of penetration depth and temperature, further increased the $\delta^{18}O_{fluid}$ between sample LP-01 and LP-04 from 4 to 7‰. This scenario is in accord with the interpretation of steam $\delta^{18}O$ variability from Panichi et al. (1974).

### 6.2. $\delta^{18}O$ variability in the Lower Reservoir and deep circulation of surficial fluids

The inter-sample textural, chemical and $\delta^{18}O$ variability of white mica from the LTGF granite reflects both their crustal source and variable extends of secondary hydrothermal alteration by infiltrating meteoric-dominated fluids. Firstly, it records the primary, magmatic signature of 10.5‰ (akin to the granitic zircon, Farina et al., 2018) that is well and homogeneously preserved in the younger granite samples CarbA-01 and -02 (both in mag and met-2 white mica), and the older, unaltered white mica in RC26B-01A (mag) (Figs. 6C–F, 7, 8). Secondly, the decrease towards lower $\delta^{18}O$ values of 4.4‰ is ascribed to the interaction with meteoric-derived water (Figs. 6–8), as found in the older granite sample RC26B-01A. These low $\delta^{18}O$ values are in equilibrium with heated surface-derived fluids with $\delta^{18}O$ of ca. 4.5‰ at 400 °C that penetrated up to 4.6 km depth (Fig. 10; Table 2). In samples from higher stratigraphic intervals, however, at temperatures below 350 °C, microscale $\delta^{18}O$ variations of up to 10‰ are preserved, despite hydrothermal alteration. This is due to microscale fluid channelling that induces precipitation of new hydrothermal white mica next to the detrital population (LP-01).

White mica from granites that experienced fluid-induced alteration at depths of 4.6 km at temperatures > 350 °C show variable decreases in $\delta^{18}O$ (Fig. 8), but also extensive recrystallization that has made white mica grains nearly homogenous in $\delta^{18}O$ at the ~100 μm scale. These results corroborate previous studies that suggested that white mica has a high reactivity, both in oxygen isotope and major element re-equilibration under hydrothermal conditions (Guidotti, 1984; Speer, 1984; Fortier and Giletti, 1991; Chacko et al., 1996; this study).

It is important to explore the correlation between white mica $\delta^{18}O$ and major (and trace) element composition to define the systematics of different chemical signals during alteration and understand the chemical exchanges during hydrothermal activity. The Ti content of the granitic white mica (both LTGF and Elba), which is commonly used as an indicator of their igneous, high-temperature origin (Miller et al., 1981; Speer, 1984; Villa et al., 1997; Cavarretta and Puxeddu, 2001; Villa et al., 2001), is generally compatible with the published range (0.01–0.04 apfu) for magmatic white mica. However, the Ti content is highly variable on intra-grain scale; in some cases it shows regular Ti zoning likely reflecting growth (Fig. 6B), and in other cases Ti zoning marks secondary replacement (Fig. 6C). In particular, the white mica in RC26B-01A displays an increase in Ti (plus Fe and Mg; Fig. 6C–D) in alteration halos around inclusions of chloritized biotite that is opposite to the expected pattern of lower Ti in altered zones. This Ti enrichment is possibly related to the liberation of Ti from biotite (≥ 2 wt% $TiO_2$; Puxeddu, 2001; Gianelli and Ruggieri, 2002) during the chloritization, since Ti is incompatible in chlorite (lower ppm range) and primarily partitions into the fluid phase (Parry and Downey, 1982; Speer, 1984). The granitic white mica also shows high values of Li and Rb (Fig. 4C–D), which are almost twice as high in white mica from CarbA-01 (up to ca. 2300 ppm each) than in the older granite RC26B-01A, supporting their different geochemical heritage.

Concomitant with the exchange of oxygen isotopes between fluid and white mica in RC26B-01A, Fe, Mg and Ti were enriched and Na slightly depleted in a halo of ≤ 40 μm around the completely chloritized biotite (Fig. 6C). Zones with higher Ti, however, show no correlation to the measured trace elements except a weak positive correlation with V. This halo of chemical alteration is also smaller than the zone of isotopic alteration. The enclosed chlorite that precipitated during the secondary, propylitic alteration is Fe-rich (27–34 wt% $FeO_{tot}$; similar to chlorite in granite intervals from MV4 and RC30 wells; Carella et al., 2000; Boyce et al., 2003) and is likely in approximate oxygen isotope equilibrium with the fluid phase (Criss and Taylor, 1986; Boyce et al., 2003). In accord with the influx of Fe and Mg with the hydrothermal fluid, the decrease in Na in these intra-grain halos is probably related to the increase in albite over K-feldspar with depth in the secondary mineral paragenesis (Boyce et al., 2003). Similar elevated Fe-Mg and lower Na values are also reported for secondary white mica in granite from other wells at the LTGF (MV7; Cavarretta and Puxeddu, 2001) and in late white mica from metasediment and contact metamorphic samples. White mica in granite sample RC26B-02E, from a similar depth to that of RC26B-01A, contains only partially chloritized or even fresh biotite and shows only a minor decrease in $\delta^{18}O$ (by ≤ 2‰) and similar Fe-Mg-Ti contents around the included biotite with respect to unaltered magmatic white mica. The magnitude of the oxygen isotope exchange experienced by the white mica is thus correlated with Fe-Mg-Ti-Na re-equilibration and the degree of chloritization (and in general propylitization) in the sample, and is indicative of the amount and the chemistry of infiltrating fluids and of the general progress of hydrothermal alteration (Parry and Downey, 1982; Criss and Taylor, 1986).

The slightly higher median $\delta^{18}O$ of CarbA versus RC26B white mica (10.5‰ to 9–10‰, Fig. 8) is compatible with their bulk rock $\delta^{18}O$ data, which shows a difference in $\delta^{18}O$ of ca. 1.5‰ (13.1‰ and 11.5‰, respectively; Gianelli and Ruggieri, 2002). In concert with their different trace element compositions – higher Li and Rb in CarbA-01 (Fig. 4D) – we interpret this difference to reflect more extensive interaction of the older RC26B granite with infiltrating hydrothermal fluids either shortly after emplacement, or later, contemporaneous with the intrusion of the younger granite bodies. Alternatively, this difference could also be a protolith inheritance, and related to their different crustal sources. The low $\delta^{18}O$ value of 2.8‰ in a recrystallized, secondary white mica grain from the strongly altered Elba granite sample CR-2 (5.9–5.4 Ma; Maineri et al., 2003; Fig. 8; Table 2), further emphasizes the relationship of intrusive age, secondary permeability and prolonged exposure to infiltrating low-$\delta^{18}O$ hydrothermal fluids.

#### 6.2.1. Mechanism for fluid infiltration

Surface-water-dominated fluids likely penetrated into the deep LR to depths of 3–5 km only through larger extensional shear zones that reach the deeper reservoir rocks of the LTGF (Brogi et al., 2003; Bellani et al., 2004; Liotta et al., 2010; Saccorotti et al., 2014). Our data show that meteoric water infiltration into the upper part of the granite and the contact aureole below is highly anisotropic, at least at sample and mineral grain scale. The contact metamorphic micaschist SP-01, for instance, comes from a depth with a p.d.T. of ca. 450 °C (Cavarretta and Puxeddu, 1990) and in this sample the met-1 white mica show homogeneous, high $\delta^{18}O$ values (9.2 ± 0.2 1σ ‰).

Since the primary permeability of the granite and the surrounding contact metamorphic rocks is inherently low, fluid infiltration is ineffective since it is likely confined to microcracks at depths of the K-horizon (4–5 km; Batini et al., 1985; Gianelli and Ruggieri, 2002; Bertini et al., 2006). It was observed that when temperatures exceed 350–370 °C there are no geothermal productive levels in the LTGF (Barelli et al., 1995). In fact Barelli et al. (1995) considered the 350 °C isotherm as the bottom of the geothermal reservoir. At this depth, close to the brittle/ductile transition, secondary permeability is low, transient and time-dependent (Baumgartner and Valley, 2001; and references therein). The critical temperature threshold for formation of effective secondary permeability in the LR is consequently < 400 °C; at these temperatures conditions change from ductile to brittle (for most strain rates), and promote active fault propagation and the formation of effective secondary permeability that allows infiltration of surficial fluids to greater depths (Bellani et al., 2004). Reaction of surface-derived fluids with the previously formed white mica in the LR (e.g., CT-01, Pad2-01, RC26B-01A) partially changed their $\delta^{18}O$ signature. This

has been shown for many minerals in contact metamorphic settings with active fluid infiltration, where increasing $\delta^{18}O$ heterogeneity towards an intrusion results from small-scale permeability differences that allow differential fluid flow into zones of higher permeability (e.g. Bowman et al., 1994; Gerdes et al., 1995a; Cook et al., 1997; Roselle et al., 1999). Stochastic permeability modelling reproduces well the heterogeneous $\delta^{18}O$ distribution and highlights the dependency that structure and permeability exert on regional and local scales on fluid-mineral exchanges in contact metamorphic aureoles (Gerdes et al., 1995b; Baumgartner and Valley, 2001). Higher temperatures, accompanied by infiltrating fluids, also increase the kinetics of recrystallization and thus the $^{18}O/^{16}O$ exchange rate (e.g. Baumgartner and Valley, 2001).

Based on published geological profiles (Fig. 7D from Bellani et al., 2004) granite sample RC26B-01A comes from a well that at 4.6 km depth is close to a large crustal shear zone, which intersects the top of the brittle-ductile transition. If, as suggested by Bertini et al. (2006), through fluid overpressure and hydrofracturing, episodic mixing between the fluid-filled microcracks and infiltrating lower-$\delta^{18}O$ fluid occurs at the depth of the brittle-ductile transition in the LTGF, the altered white mica in granite sample RC26B-01A should record such a fluid mixing episode. It is conceivable that based on the high ambient temperature and the time between high strain episodes, this entrapped fluid could partially equilibrate, for instance, with the enclosing white mica and lower the mineral $\delta^{18}O$. However, it is more likely that < 400 °C temperatures at depth in the older Radicondoli intrusion promoted the deep infiltration of meteoric-derived fluids through fracture-induced secondary permeability and thus selectively lowered the $\delta^{18}O$ of white mica. On the contrary, the higher temperatures in the younger Carboli intrusion prevented permeability and fluid infiltration and thus preserved homogeneous, high $\delta^{18}O$ white mica.

### 6.3. K-Ar age variability in hydrothermal white mica and spatial infiltration patterns of surficial fluids

At present, the inventory of known granitic intrusions in the LTGF totals about 14 and contact metamorphic minerals have been dated in another 4 wells. The chronology of these events shows resolvable differences (see Table 4).

Contact metamorphic and hydrothermal white mica that either do not occur in immediate proximity to a known granite or post-date the ages of the magmatic mica generation that coexists with it have been dated in wells Canneto 4A (CT-01, 4.2 Ma: this work), Larderello Profondo (LP-01, ≤4 Ma: this work), Sasso 22 (3.0–3.5 Ma: Del Moro et al., 1982), Padule 2 (2.0 Ma and ≤1.3 Ma: this work), San Pompeo (1.6 Ma: Villa and Puxeddu, 1994), and Carboli C bis (0.7 Ma: Villa et al., 2001). At the SE edge of the presently active LTGF, the Boccheggiano fossil geothermal field (Rossetti et al., 2008) shows evidence of HT contact metamorphism by a hidden intrusion. Its retrograde evolution is characterized by the progressive development of a composite D3-D4 fabric and likely lasted from 2.8 ± 0.1 Ma (D3 phase) to ca. 0.7 Ma (Rossetti et al., 2008).

**Table 4**
Ages of cored granitoids in the Larderello-Travale Geothermal Field.

| Well | Age (Ma) | Referencesa |
|---|---|---|
| Monteverdi 7 | 3.8 | VP94 |
| MTR | 3.7 | Fa18 |
| Montieri 7 mid | 3.3 | Vi06 |
| Montieri 7 top | 3.1 | Vi06 |
| VC11 | 2.9 | VP94 |
| Radicondoli 26 | 2.7 | Vi97; Fa18; tw |
| Montieri 7 bottom | 2.7 | Vi06 |
| Chiusdino mid | 2.6 | Vi06 |
| Chiusdino bottom | 2.6 | Vi06 |
| Travale Sud | 2.6 | Vi06; Fa18 |
| Radicondoli 29 | 2.3 | GL01 |
| Chiusdino top | 2.3 | Vi06 |
| Carboli C bis | 1.7 | Vi01; Fa18 |

Reference abbreviations: Fa18, Farina et al., 2018; GL01, Gianelli and Laurenzi, 2001; tw, this work; Vi97, Villa et al., 1997; Vi01, Villa et al., 2001; Vi06, Villa et al., 2006; VP94, Villa and Puxeddu, 1994.

Dini et al. (2005) defined two broad magmatic pulses in a 100 $km^2$ area in and around the LTGF: (1) between 3.8 and 3.5 Ma, with a tail extending towards 3.0 Ma, and (2) between 2.9 and 2.5 Ma, with isolated intrusions between 2 and 1.7 Ma. However, these apparent peaks may very well be sampling biases, as the general pattern is that these granites are relatively small (ca. 1 $km^3$) and each is clearly distinct from its immediate neighbours (Dini et al., 2005; Villa et al., 2006; Farina et al., 2018). It is likely that the hydrothermal circulation events whose ages do not match a known nearby granite intrusion were powered by other, as yet unidentified granitoid intrusions.

The K-horizon, a (micro)fracture-bound, fluid-rich level on top of the younger, Quaternary granite intrusions, is a present-day feature that discontinuously extends across the entire LTGF. Our age data, in accordance with the $\delta^{18}O$ data, require that the meteoric water infiltration pattern was not only patchy at the mm scale (producing the observed $\delta^{18}O$ variations described above) but also at the km scale, as attested by the 2 Ma age difference between hydrothermal white mica in the two wells – Pad2-01 and CT-01 – 2 km apart (Fig. 1A). This spatially heterogeneous influx can be attributed to sub-vertical fractures that channelled meteoric waters as far as the LR at different times in different places.

### 6.4. Microscale $\delta^{18}O$ variability and their geothermal implications

The two major observations from the UR and LR are that some sampled intervals contain white mica with homogeneous $\delta^{18}O$ values, whereas other intervals have white micas with pronounced microscale $\delta^{18}O$ heterogeneity (Fig. 8). The heterogeneity in oxygen isotopes (and K−Ar ages), is however not necessarily correlated with the white mica chemistry, although a trend towards higher Si and Mg, as well as lower Na contents in hydrothermally altered, lower-$\delta^{18}O$ white mica is detected (e.g., LP-01, RC26B-01A; Fig. 7). The addition of Si and Mg (± Fe, Ti) follows the Tschermak exchange and likely reflects the progressive enrichment of these elements in the fluid during penetration in the hydrothermal system. A structural example of this element mobility in fluids that supports the hydrothermal fluid channelling hypothesis is the mineralized Boccheggiano extensional fault (Liotta et al., 2010; Rossetti et al., 2011). Here fluids of dominantly meteoric origin ($\delta^{18}O$ of ca. –5.7 to 0‰) produced epithermal, polycyclic sulphide mineralization in an extensional regime with fluid-pressure fluctuations as key control on the fault permeability. The selective, diachronous fluid alteration and thus the variably low $\delta^{18}O$ values in, for instance, secondary quartz, have been attributed to the anisotropic permeability of the Boccheggiano fault zone (Brogi et al., 2003; Bellani et al., 2004; Liotta et al., 2010; Rossetti et al., 2011).

In our samples, the HT veins (Pad2-01 and CT-01) likely represent filled remnants of earlier micro-hydrofractures, similar to the ones described by Barelli et al. (2000) for other wells intersecting granite in the LTGF. The very selective $\delta^{18}O$ alteration, recorded in white mica from the UR and LR alike, is evidenced by the white micas in the HT veins of CT-01 and Pad2-01 (both ≥2.7 km depth), which show the highest intra- and inter-grain $\delta^{18}O$ variation of all sampled intervals (Fig. 8). This microscale variability of up to 10‰ (Fig. 5C–D, 6 A–B; CT-01 and Pad2-01) indicates that crystallographic-controlled diffusional homogenization is effectively absent at the p.d.T. below ca. 350 °C in the samples. The lack of oxygen isotope exchange below 350 °C froze the variable $\delta^{18}O$ signature of the large met-2 white micas dated at 4 Ma (CT-01) and 2 Ma (Pad2-01). White mica from the host rock around the vein in CT-01, also shows low $\delta^{18}O$ of ca. 2‰ in a small grain (< 100 μm) associated with K-feldspar and biotite (both low closure

temperature; Kohn and Valley, 1998). Unlike the large grains in the veins, this small grain likely recrystallized completely in equilibrium with a fluid of 1 to 3‰ (based on minimum p.d.T. of 320 °C and probable maximum T of 500 °C, respectively). Besides the age difference of 2 Myr between white mica in the two HT veins, further information on the fluid source for these samples comes from their trace element composition. Although white mica from both vein samples from Pad2-01 and CT-01 show comparable trace element patterns (Fig. 4C), significant differences are observed for Li and Ba. White mica from the HT vein sample Pad2-01 has higher Li values, likely through their precipitation from Li-B-rich magmatic fluids, also with higher overall $\delta^{18}O$ values (Fig. 8). Their low B values are likely due to the co-precipitation with tourmaline (Fig. 3H). In contrast, white mica from the small vein in micaschist CT-01, has low Li and Rb values, suggesting minor interaction with magmatic fluids. However, Ba contents are very high with up to 6700 ppm (Fig. 4E–F), especially in the host rock white mica in CT-01, and in accord with their low $\delta^{18}O$ values (ca. 2‰) this could be another indication for their interaction with surficial, UR waters. Surface-derived fluids in the LTGF contain Ba due to interaction with the carbonate-evaporite sequences in the UR (Cavarretta et al., 1982). These observations are also consistent with the temperature – secondary permeability dependence discussed above for the granite samples and published fluid inclusion data (Cathelineau et al., 1994; Boiron et al., 2007). Initial formation of the HT vein white mica was during an intrusive or contact metamorphic episode and after cooling of the system below 400 °C, surficial-derived fluids interacted at various degrees with the vein and host rock white mica and variably lowered their $\delta^{18}O$ values.

In summary, $^{18}O/^{16}O$, trace element and K-Ar age variability occurs in zones of higher secondary permeability (at temperatures < 400 °C), both on regional and local scale, such as contact metamorphic micaschist (CT-01), HT veins in the vicinity of the granitic intrusions (Pad2-01) and in the intrusions themselves if intersected by fault zones (RC26B-01A). The $\delta^{18}O$ signature in these LR white mica grains then indicates that effective infiltration and episodic mixing of UR fluids with LR fluids occurs in vicinity of the K-horizon and the deep-seated geothermal reservoir at the LTGF.

## 7. Conclusions

The new microscale $\delta^{18}O$ values and age data of white mica at the LGTF reveal that:

1. $^{18}O/^{16}O$ exchange in white mica is the result of recrystallization (e.g. LP-01, RC26B) in the presence of a fluid phase with variable chemistry,
2. variability in $\delta^{18}O$ values is not necessarily correlated to major or trace element variability (e.g. CT-01, Pad2-01),
3. several per mil $^{18}O/^{16}O$ variability ("disequilibrium") occurs and persists at the µm-scale in an active geothermal field at various depths and at present-day temperatures up to 350 °C on inter-grain (depth of 581 m and 3523 m) and intra-grain scale (depth of 2782 m, 3523 m, 4600 m),
4. oxygen isotope re-equilibration via diffusive exchange in white mica is insignificant at temperatures below ca. 350 °C over millions of years (4 Ma in CT-01, 2 Ma in Pad2-01),
5. key factors controlling the extent of oxygen isotope exchange in white mica from the LTGF are temperature (a primary control on the rate of recrystallization) and the extend of fluid infiltration and fluid – white mica interaction enabled by the secondary (regional and local) permeability of the system,
6. localized infiltration of meteoric fluids occurs with little fluid-rock interaction along sub-vertical faults, fractures and cleavages down to ca. 4.6 km. These fluids infiltrate anisotropically through the reservoir host rocks and thus selectively alter white mica isotopically and/or chemically at different times in different places at spatial scales down to < 100 µm,
7. $^{39}Ar$-$^{40}Ar$ age data record this diachroneity between hydrothermal white mica cored in different, but spatially proximal localities (CT-01, Pad2-01).

Supplementary data to this article can be found online at https://doi.org/10.1016/j.chemgeo.2019.119288.

## Acknowledgements

The authors would like to thank Enel Green Power S.p.A. for providing the well samples from the Larderello geothermal field and the permission to publish the results. Thanks are also due to P. Lanari for assistance with the EPMA and F. Piccoli for help with the Laser-ICP-MS. We are also thankful for constructive reviews by J. Bowman, F. Farina and C. Harris that helped to improve the manuscript. This research was supported by the Swiss National Science Foundation – projects 200021_166280 and 206021_170722.

## References

Airaghi, L., Lanari, P., de Sigoyer, J., Guillot, S., 2017. Microstructural vs compositional preservation and pseudomorphic replacement of muscovite in deformed metapelites from the Longmen Shan (Sichuan, China). Lithos 282, 262–280.
Barelli, A., Cappetti, G., Stefani, G., 1995. Results of deep drilling in the Larderello-Travale/Radicondoli geothermal area. Proc. World Geothermal Congress 1275–1278.
Barelli, A., Bertini, G., Buonasorte, G.C., Fiordelisi, A., 2000. Recent deep exploration results at the margins of the Larderello Travale Geothermal System. Proc. World Geothermal Congress 965–970.
Batini, F., Bertini, G., Gianelli, G., Pandeli, E., Puxeddu, M., Villa, I.M., 1985. Deep structure, age and evolution of the Larderello-Travale geothermal field. Geothermal Resources Council Transactions 9, 253–259.
Baumgartner, L.P., Valley, J.W., 2001. Stable isotope transport and contact metamorphic fluid flow. In: In: Valley, J.W., Cole, D.R. (Eds.), Stable Isotope Geochemistry. Rev. Mineral, vol. 43. pp. 415–467.
Bellani, S., Brogi, A., Lazzarotto, A., Liotta, D., Ranalli, G., 2004. Heat flow, deep temperatures and extensional structures in the Larderello Geothermal Field (Italy): constraints on geothermal fluid flow. J. Volcanol. Geoth. Res. 132, 15–29.
Bertini, G., Casini, M., Gianelli, G., Pandeli, E., 2006. Geological structure of a long-living geothermal system, Larderello, Italy. Terra Nova 18, 163–169.
Bindeman, I., 2008. Oxygen isotopes in mantle and crustal magmas as revealed by single crystal analysis. In: K.D., Putirka, F.J., Tepley III (Editors), Minerals, Inclusions and Volcanic Processes. Rev. Mineral. Geochem. 69, 445–478.
Boiron, M.C., Cathelineau, M., Ruggieri, G., Jeanningros, A., Gianelli, G., Banks, D.A., 2007. Active contact metamorphism and $CO_2$–$CH_4$ fluid production in the Larderello geothermal field (Italy) at depths between 2.3 and 4 km. Chem. Geol. 237, 303–328.
Bottinga, Y., Javoy, M., 1973. Comments on oxygen isotope geothermometry. Earth Planet. Sci. Lett. 20, 250–265.
Bowman, J.R., Willett, S.D., Cook, S.J., 1994. Oxygen isotope transport and exchange during fluid flow: Onedimensional models and applications. Am. J. Sci. 294, 1–55.
Boyce, A.J., Fulignati, P., Sbrana, A., 2003. Deep hydrothermal circulation in a granite intrusion beneath Larderello geothermal area (Italy): constraints from mineralogy, fluid inclusions and stable isotopes. J. Volcanol. Geoth. Res. 126, 243–262.
Brogi, A., Lazzarotto, A., Liotta, D., Ranalli, G., 2003. Extensional shear zones as imaged by reflection seismic lines: the Larderello geothermal field (Central Italy). Tectonophysics 363, 127–139.
Carella, M., Fulignati, P., Musumeci, G., Sbrana, A., 2000. Metamorphic consequences of Neogene thermal anomaly in the Northern Apennines (Radicondoli-Travale area, Larderello geothermal field-Italy). Geodyn. Acta 13, 345–366.
Casini, M., Ciuffi, S., Fiordelisi, A., Mazzotti, A., Stucchi, E., 2010. Results of a 3D seismic survey at the Travale (Italy) test site. Geothermics 39, 4–12.
Cathelineau, M., Marignac, C., Boiron, M.C., Gianelli, G., Puxeddu, M., 1994. Evidence for Li-rich brines and early magmatic fluid-rock interaction in the Larderello geothermal system. Geochim. Cosmochim. Acta 58, 1083–1099.
Cavarretta, G., Puxeddu, M., 1990. Schorl-dravite-ferridravite tourmalines deposited by hydrothermal magmatic fluids during early evolution of the Larderello geothermal field. Econ. Geol. 85, 1236–1251.
Cavarretta, G., Puxeddu, M., 2001. Two-mica F–Li–B-rich monzogranite apophysis of the Larderello batholith cored from 3. 5 km depth. N. Jb. Miner. Abh. 177, 77–112.
Cavarretta, G., Gianelli, G., Puxeddu, M., 1980. Hydrothermal metamorphism in the Larderello geothermal field. Geothermics 9, 297–314.
Cavarretta, G., Gianelli, G., Puxeddu, M., 1982. Formation of authigenic minerals and their use as indicators of the physicochemical parameters of the fluid in the Larderello-Travale geothermal field. Econ. Geol. 77, 1071–1084.
Celati, R., Noto, P., Panichi, C., Squarci, P., Taffi, L., 1973. Interactions between the steam reservoir and surrounding aquifers in the Larderello Geothermal Field. Geothermics 2, 174–185.
Chacko, T., Xiansheng, H., Mayeda, T.K., Clayton, R.N., Goldsmith, J.R., 1996. Oxygen isotope fractionations in muscovite, phlogopite, and rutile. Geochim. Cosmochim. Acta 60, 2595–2608.
Cook, S.J., Bowman, J.R., Forster, C.B., 1997. Contact metamorphism surrounding the Alta stock: finite element model simulation of heat- and $^{18}O/^{16}O$ mass-transport

during prograde metamorphism. Am. J. Sci. 297, 1–55.
Criss, R.E., Taylor, H.P., Taylor Jr., H.P., 1986. Meteoric-hydrothermal systems. In: In: Valley, J.W., O'Neil, J.R. (Eds.), Stable Isotopes in High Temperature Geological Processes, vol. 16. pp. 373–427.
Dallai, L., Magro, G., Petrucci, E., Ruggieri, G., 2005. Stable isotope and noble gas isotope compositions of inclusion fluids from Larderello geothermal field (Italy): Constraints to fluid origin and mixing processes. J. Volcanol. Geoth. Res. 148, 152–164.
D'Amore, F., Bolognesi, L., 1994. Isotopic evidence for a magmatic contribution to fluids of the geothermal systems of Larderello, Italy, and the Geysers, California. Geothermics 23, 21–32.
D'Amore, F., Fancelli, R., Panichi, C., 1987. Stable isotope study of reinjection processes in the Larderello geothermal field. Geochim. Cosmochim. Acta 51, 857–867.
Del Moro, A., Puxeddu, M., Radicati di Brozolo, F., Villa, I.M., 1982. Rb–Sr and K–Ar ages on minerals at temperature of 300 – 400°C from deep wells in the Larderello geothermal field, Italy. Contrib. Miner. Petrol. 81, 340–349.
Dini, A., Gianelli, G., Puxeddu, M., Ruggieri, G., 2005. Origin and evolution of Pliocene-Pleistocene granites from the Larderello geothermal field (Tuscan Magmatic Province, Italy). Lithos 81, 1–31.
Dini, A., Mazzarini, F., Musumeci, G., Rocchi, S., 2008. Multiple hydro-fracturing by boron-rich fluids in the Late Miocene contact aureole of eastern Elba Island (Tuscany, Italy). Terra Nova 20, 318–326.
Eiler, J.M., 2001. Oxygen isotope variations of basaltic lavas and upper mantle rocks. In: In: Valley, J.W., Cole, D.R. (Eds.), Stable Isotope Geochemistry, vol. 43. pp. 319–364.
Eiler, J.M., Valley, J.W., Baumgartner, L.P., 1993. A new look at stable isotope thermometry. Geochim. Cosmochim. Acta 57, 2571–2583.
Farina, F., Dini, A., Ovtcharova, M., Davies, J.H.F.L., Greber, N.D., Bouvier, A.S., Baumgartner, L., Ulianov, A., Schaltegger, U., 2018. Zircon petrochronology reveals the timescale and mechanism of anatectic magma formation. Earth Planet. Sci. Lett. 495, 213–223.
Ferry, J.M., Kitajima, K., Strickland, A., Valley, J.W., 2014. Ion microprobe survey of the grain-scale oxygen isotope geochemistry of minerals in metamorphic rocks. Geochim. Cosmochim. Acta 144, 403–433.
Fortier, S.M., Giletti, B.J., 1991. Volume self-diffusion of oxygen in biotite, muscovite, and phlogopite micas. Geochim. Cosmochim. Acta 55, 1319–1330.
Gerdes, M.L., Baumgartner, L.P., Person, M., Rumble, D., 1995a. One- and two-dimensional models of fluid flow and stable isotope exchange at an outcrop in the Adamello contract aureole, Southern Alps, Italy. Am. Mineral. 80, 1004–1019.
Gerdes, M.L., Baumgartner, L.P., Person, M., 1995b. Stochastic permeability models of fluid flow during contact metamorphism. Geology 23, 945–948.
Gianelli, G., Laurenzi, M.A., 2001. Age and cooling rate of the geothermal system of Larderello. Geoth. Res. T. 25, 731–735.
Gianelli, G., Ruggieri, G., 2002. Evidence of a contact metamorphic aureole with high-temperature metasomatism in the deepest part of the active geothermal field of Larderello, Italy. Geothermics 31, 443–474.
Gianelli, G., Ruggieri, G., Mussi, M., 1997. Isotopic and fluid inclusion study of hydrothermal and metamorphic carbonates in the Larderello geothermal field and surrounding areas, Italy. Geothermics 393–417.
Gianelli, G., Puxeddu, M., Ruggieri, G., 2001. Contents of F, Cl, Li and B in the granite intrusions of Larderello, Italy. In: Cidu, R. (Ed.), Water-Rock Interaction 2001. Balkema, Lisse, pp. 842–939.
Guidotti, C.V., 1984. Micas in metamorphic rocks. In: In: Bailey, S.W. (Ed.), Micas. Rev. Mineral, vol. 13. pp. 357–467.
Kita, T.N., Ushikubo, T., Fu, B., Valley, J.W., 2009. High precision SIMS oxygen isotope analysis and the effect of sample topography. Chem. Geol. 264, 43–57.
Kohn, M.J., Valley, J.W., 1998. Obtaining equilibrium oxygen isotope fractionations from rocks: theory and examples. Contrib. Mineral. Petrol. 132, 209–224.
Lacroix, B., Vennemann, T., 2015. Empirical calibration of the oxygen isotope fractionation between quartz and Fe-Mg-chlorite. Geochim. Cosmochim. Acta 149, 21–31.
Liotta, D., Ruggieri, G., Brogi, A., Fulignati, P., Dini, A., Nardini, I., 2010. Migration of geothermal fluids in extensional terrains: the ore deposits of the Boccheggiano-Montieri area (southern Tuscany, Italy). Int. J. Earth Sci. 99, 623–644.
Lanari, P., Vidal, O., De Andrade, V., Dubacq, B., Lewin, E., Grosch, E.G., Schwartz, S., 2014. XMapTools: A MATLAB©-based program for electron microprobe X-ray image processing and geothermobarometry. Comput. Geosci. 62, 227–240.
Luisier, C., 2018. Pressure Variations in the Monte Rosa Nappes, Western Alps. Université de Lausanne, Faculté des géosciences et de l'environnement (unpublished PhD. Thesis). Open repository. https://serval.unil.ch/resource/serval:BIB_119C18C15763.P001/REF.
Maineri, C., Benvenuti, M., Costagliola, P., et, a., 2003. Sericitic alteration at the La Crocetta deposit (Elba Island, Italy): interplay between magmatism, tectonics and hydrothermal activity. Miner. Depos. 38, 67–86.
Miller, C.F., Stoddard, E.F., Bradfish, L.J., Dollase, W.A., 1981. Composition of plutonic muscovite: Genetic implications. Can. Mineral. 19, 25–34.
Montemagni, C., Montomoli, C., Iaccarino, S., et al., 2018. Dating protracted fault activities: microstructures, microchemistry and geochronology of the Vaikrita Thrust, Main Central Thrust zone, Garhwal Himalaya, NW India. Geol. Soc. Spec. Publ. 481. https://doi.org/10.1144/SP481.3.
Musumeci, G., Bocini, L., Corsi, R., 2002. Alpine tectonothermal evolution of the Tuscan Metamorphic complex in the Larderello geothermal field (northern Apennines, Italy). J. Geol. Soc. Lond. 159, 443–456.
O'Neil, J.R., Taylor, H.P., 1969. Oxygen isotope equilibrium between muscovite and water. J. Geophys. Res. Atmos. 74, 6012–6022.
Pandeli, E., Gianelli, G., Morelli, M., 2005. The crystalline units of the middle-upper crust of the Larderello geothermal region (southern Tuscany, Italy): new data for their classification and tectono-metamorphic evolution. Boll. Soc. Geol. It. 3, 139–155.
Panichi, C., Celati, R., Noto, P., Squarci, P., Taffi, L., Tongiorgi, E., 1974. Oxygen and hydrogen isotope studies of the Larderello (Italy) geothermal system. In: Isotope Techniques in Groundwater Hydrology 1974, Vol. 2. I.A.E.A Vienna, Austria. pp. 3–28.
Panichi, C., Scandiffio, G., Baccarin, F., 1995. Variation of geochemical parameters induced by reinjection in the Larderello area. Proc. World Geothermal Congress 1845–1849.
Parri, R., Lazzeri, F., 2016. Larderello; 100 years of geothermal power plant evolution in Italy. In: DiPippo, R. (Ed.), Geothermal Power Generation – Developments and Innovation. Elsevier, Amsterdam, pp. 537–590.
Parry, W.T., Downey, L.M., 1982. Geochemistry of hydrothermal chlorite replacing igneous biotite. Clay Clay Miner. 30, 81–90.
Paton, C., Hellstrom, J., Paul, B., Woodhead, J., Hergt, J., 2011. Iolite: Freeware for the visualisation and processing of mass spectrometric data. J. Anal. At. Spectrom. 26, 2508.
Petrucci, E., Sheppard, S.M.F., Turi, B., 1993. Water/rock interaction in the Larderello geothermal field (southern Tuscany, Italy): an $^{18}O/^{16}O$ and D/H isotope study. J. Volcanol. Geoth. Res. 59, 145–160.
Petrucci, E., Gianelli, G., Puxeddu, M., Iacumin, P., 1994. An oxygen isotope study of silicates at Larderello, Italy. Geothermics 23, 327–337.
Pettke, T., Oberli, F., Audetat, A., et al., 2012. Recent developments in element concentration and isotope ratio analysis of individual fluid inclusions by laser ablation single and multiple collector ICP-MS. Ore Geol. Rev. 44, 10–38.
Puxeddu, M., Squarci, P., Rau, A., Tongiorgi, M., Burgassi, B.D., 1977. Stratigraphic and tectonic study of Larderello-Travale basement rocks and its geothermal implications. Geothermics 6, 83–93.
Puxeddu, M., Saupé, F., Déchomets, R., Gianelli, G., Moine, B., 1984. Geochemistry and stratigraphic correlations—application to the investigation of geothermal and mineral resources of Tuscany, Italy. Chem. Geol. 43, 77–113.
Rieder, M., Cavazzini, G., et al., 1998. Nomenclature of the micas. Can. Mineral. 36, 902–912.
Roselle, G.T., Baumgartner, L.P., Valley, J.W., 1999. Stable isotope evidence of heterogeneous fluid infiltration at the Ubehebe Peak contact aureole, Death Valley National Park, California. Am. J. Sci. 299, 93–138.
Rossetti, F., Balsamo, F., Villa, I.M., Boujbauenne, M., Faccenna, C., Funiciello, R., 2008. Pliocene–Pleistocene HT/LP metamorphism during multiple granitic intrusions in the southern branch of the Larderello geothermal field (southern Tuscany, Italy). J. Geol. Soc. Lond. 165, 247–262.
Rossetti, F., Aldega, L., Tecce, F., Balsamo, F., Billi, A., Brilli, M., 2011. Fluid flow within the damage zone of the Boccheggiano extensional fault (Larderello–Travale geothermal field, central Italy): structures, alteration and implications for hydrothermal mineralization in extensional settings. Geol. Mag. 148, 558–579.
Roumé jon, S., Williams, M.J., Früh-Green, G.L., 2018. In-situ oxygen isotope analyses in serpentine minerals: Constraints on serpentinization during tectonic exhumation at slow- and ultraslow-spreading ridges. Lithos 323, 156–173.
Rudnick, R.L., Gao, S., 2004. Composition of the Continental Crust. In: In: Holland, H.D., Turekian, K.K. (Eds.), Treatise on Geochemistry, vol. 3. Elsevier, Amsterdam, pp. 1–64.
Ruggieri, G., Gianelli, G., 1999. Multi-stage fluid circulation in a hydraulic fracture breccia of the Larderello geothermal field, Italy. J. Volcanol. Geoth. Res. 90, 241–261.
Ruggieri, G., Cathelineau, M., Boiron, M.C., Marignac, C., 1999. Boiling and fluid mixing in the chlorite zone of the Larderello geothermal field. Chem. Geol. 154, 237–256.
Saccorotti, G., Piccinini, D., Zupe, M., et al., 2014. The deep structure of the Larderello-Travale geothermal field (Italy) from integrated, passive seismic investigations. Energy Procedia 59, 227–234.
Scicchitano, M.R., Rubatto, D., Hermann, J., et al., 2018. In situ oxygen isotope determination in serpentine minerals by ion microprobe: reference materials and applications to Ultrahigh-pressure Serpentinites. Geostand. Geoanalytical Res. 42, 459–479.
Sheppard, S.M.F., 1986. Characterization and isotopic variations in natural waters. In: In: Valley, J.W., Taylor Jr.H.P., O'Neil, J.R. (Eds.), Stable Isotopes in High Temperature Geological Processes, vol. 16. pp. 165–183.
Siron, G., Baumgartner, L., Bouvier, A.-S., Putlitz, B., Vennemann, T., 2017. Biotite reference materials for secondary ion mass spectrometry $^{18}O/^{16}O$ measurements. Geostand. Geoanalytical Res. 41, 243–253.
Speer, J.A., 1984. Micas in igneous rocks. In: In: Bailey, S.W. (Ed.), Micas. Rev. Mineral, vol. 13. pp. 299–356.
Taylor, H.P.J., 1977. Water/rock interactions and the origin of H2O in granitic batholiths. J. Geol. Soc. Lond. 133, 509–558.
Taylor, H.P.J., Sheppard, S.M.F., 1986. Igneous rocks: I. Processes of isotopic fractionation and isotope systematics. In: In: Valley, J.W., Taylor Jr.H.P., O'Neil, J.R. (Eds.), Stable Isotopes in High Temperature Geological Processes, vol. 16. pp. 227–272.
Taylor, H.P.J., Turi, B., 1976. High $^{18}O$ igneous rocks from the Tuscan magmatic Province, Italy. Contrib. Mineral. Petrol. 55, 1–31.
Valley, J.W., 1986. Stable isotope geochemistry of metamorphic rocks. In: J.W. Valley, H. P. Taylor Jr. and J.R. O'Neil (Editors), Stable Isotopes in High Temperature Geological Processes. Rev. Mineral. vol. 16, 445–486.
Valori, A., Cathelineau, M., Marignac, Ch., 1992. Early fluid migration in a deep part of the Larderello geothermal field: a fluid inclusion study of the granite sill from well Monteverdi. J. Volcanol. Geoth. Res. 51, 115–131.
Villa, I.M., Hanchar, J.M., 2017. Age discordance and mineralogy. Am. Mineral. 102, 2422–2439.
Villa, I.M., Puxeddu, M., 1994. Geochronology of the Larderello geothermal field: new data and the "closure temperature" issue. Contrib. Mineral. Petrol. 115, 415–426.
Villa, I.M., Gianelli, G., Puxeddu, M., Bertini, G., Pandeli, E., 1987. Granitic dykes of 3.8 Ma age from a 3.5 km deep geothermal well at Larderello (Italy). Rend. Soc. Ital.

Mineral. Petrol. 42, 364.
Villa, I.M., Ruggieri, G., Puxeddu, M., 1997. Petrological and geochronological discrimination of two white-mica generations in a granite cored from the Larderello-Travale geothermal field (Italy). Eur. J. Mineral. 9, 563–568.
Villa, I.M., Ruggieri, G., Puxeddu, M., 2001. Geochronology of Magmatic and Hydrothermal Micas from the Larderello Geothermal Field, Italy. Cidu, Rosa Water Rock Interaction. Balkema Publishers, Lisse, pp. 1589–1592.
Villa, I.M., Ruggieri, G., Puxeddu, M., Bertini, G., 2006. Geochronology and isotope transport systematics in a subsurface granite from the Larderello–Travale geothermal system (Italy). J. Volcanol. Geotherm. Res. 152, 20–50.
Wedepohl, K.H., 1995. The composition of the continental crust. Geochim. Cosmochim. Acta 59, 1217–1239.
Zheng, Y.-F., 1993. Calculation of oxygen isotope fractionation in hydroxyl-bearing silicates. Earth Planet. Sci. Lett. 120, 247–263.
Zucchi, M., Brogi, A., Liotta, D., et al., 2017. Permeability and hydraulic conductivity of faulted micaschist in the eastern Elba Island exhumed geothermal system (Tyrrhenian Sea, Italy): insights from Cala Stagnone. Geothermics 70, 125–145.